Sound & Vibration 2026, 60(4), 4262.
doi: https://doi.org/10.59400/sv4262

Article

Co-design of mechanical and electrical parameters in wind turbine gearbox-generator systems

Ruibo Chen[1,2,3,*], Zhonghua Wu[1], Jinwei Sun[2], Datong Qin[3], Chuanwei Zhao[1]

[1] Drilling Technology Research Institute of Shengli Petroleum Engineering Corporation, Sinopec, Dongying 257017, China
[2] Department of Instrumentation Science and Engineering, Harbin Institute of Technology, Harbin 150001, China
[3] State Key Laboratory of Mechanical Transmission for Advanced Equipment, Chongqing University, Chongqing 400044, China
*** Corresponding author:** Ruibo Chen, chenruibo1993@163.com

CITATION

Chen R, Wu Z, Sun J, et al. Co-design of mechanical and electrical parameters in wind turbine gearbox-generator systems. Sound & Vibration. 2026; 60(4): 4262. https://doi.org/10.59400/sv4262

ARTICLE INFO

Received: 13 April 2026
Revised: 10 May 2026
Accepted: 15 May 2026
Available online: 20 July 2026

Abstract: Conventional design practices for wind turbine drivetrains commonly adopt a segregated workflow where the gearbox and electrical machine are developed independently. Such a decoupled strategy overlooks inherent electromechanical coupling constraints, thereby imposing fundamental limits on attainable power density and dynamic behavior of the entire transmission assembly. To mitigate these limitations, this work presents a hierarchical integrated parameter co-design framework for wind turbine gearbox–generator systems, which implements progressive optimization from system-level to component-level, while synchronously satisfying static performance and dynamic response requirements. In the first design stage, an integrated initial parameterization scheme is formulated via finite element analysis (FEA) and numerical computation, with objectives to elevate system power density and suppress amplitudes of internal dynamic excitations. The optimized parameters from this stage serve as baseline inputs for the second stage. An electromechanically coupled dynamic model is then established to quantify correlations between key mechanical structural parameters (gearbox bearings, hollow shafts, splines, ring gear bolt stiffness) and generator electromagnetic/structural parameters, as well as overall system dynamic characteristics. Sensitive design variables are identified via correlation analysis, and a Kriging surrogate model is constructed to approximate nonlinear input–output relationships efficiently. Multi-objective component optimization is subsequently performed using the surrogate model. Finally, vibration attenuation and load reduction performances of the baseline and optimized drivetrain configurations are systematically compared under rated and variable operating conditions.

Keywords: wind turbine transmission system; electromechanical coupling dynamic model; electromechanical coupling dynamic characteristics; electromechanical integration design

1. Introduction

Driven by global carbon peaking and carbon neutrality strategies, wind energy has become one of the most promising renewable energy sources and a strategically important industry worldwide. As wind turbines continue to develop toward large-scale and high-power levels, the volume and weight of gearbox–generator units increase significantly, which increases the load on the tower and brings inconvenience to installation and maintenance. Therefore, reducing the volume and weight of the transmission system and improving power density have become important development goals. At the same time, optimizing dynamic load characteristics is also critical to enhance stability and service life.

Substantial research has been conducted on the design parameters of gearboxes, with particular emphasis on optimizing their volume, weight, and power density. Rubio et al. [1] analyzed the influence of calculation parameters, such as the module and tooth width, on the size and weight of a high-power wind turbine epicyclic gearbox following ISO 6336, providing a theoretical basis for achieving more compact and lighter designs. Similarly, Llopis-Albert et al. [2] developed a digital twin-based multi-objective optimization framework that integrates CAD/CAE tools to minimize the weight, volume, and maximum stresses of wind turbine gearboxes without compromising efficiency. Their work highlights the trade-offs between competing design variables to enhance power density. Wang [3] introduced a high power density design approach for a helical differential gear train by studying its dynamic performance, successfully reducing power loss and volume while improving vibration characteristics. Bußkamp et al. [4] presented a multiobjective optimization method focused on the micro-geometry of the high-speed shaft components to reduce the risk of gear and bearing damage during transient grid faults. Zhou et al. [5] developed a gear transmission optimization model aimed at minimizing gear center distance while improving gearbox load capacity, leading to mass reduction via multi-objective optimization algorithms. Savsani et al. [6] applied both the ant colony and simulated annealing algorithms to the lightweight design of a gear transmission system, noting that the simulated annealing method provided faster and more accurate solutions. Gologlu and Zeyveli [7] minimized the total volume of a gear transmission system using a genetic algorithm and a penalty function method. Chen et al. [8] used a hybrid genetic algorithm for lightweight design of a single straight-cylinder gear reducer. Wei et al. [9] conducted multi-objective optimization of a multi-power planetary transmission system, aiming to minimize total volume and variation in gear strength safety factors across stages. Liang et al. [10] performed lightweight topology optimization of a gearbox based on the variable density method, using multi-condition strain energy as the objective and volume as the constraint. Lv et al. [11] studied a 2 MW wind turbine transmission system, performing sensitivity analysis on elastic support stiffness using ABAQUS and Isight, followed by stiffness parameter optimization. In summary, the studies referenced above primarily focus on improving the power density of wind turbine gearboxes and assessing system reliability from a static perspective, largely overlooking dynamic performance considerations.

Many scholars have investigated the dynamic performance and reliability optimization of wind turbine gearboxes. Among them, Lei et al. [12] developed a hybrid finite element and Hertz contact model for analyzing helical gear load contact. To reduce transmission vibration and improve durability, a multi-objective optimization model was established, which was then converted into a single-objective problem via a weighting coefficient method and solved using a particle swarm optimization algorithm to determine optimal gear modification parameters. Jouilel et al. [13] constructed an uncertain physical model based on bond graph theory for a 750 kW horizontal-axis wind turbine gearbox. A comprehensive parameter identification across variation intervals was conducted using Monte Carlo simulation, leading to improved efficiency of the electromechanical transmission system. Bozca [14] aimed to reduce system excitation by minimizing gear transmission error fluctuation. Using the peak-to-peak transmission error as the target, the gear transmission parameters were optimized via sequential quadratic programming, resulting in a 10% reduction in gear rattling noise. Garambois et al. [15] treated transmission error and mesh stiffness fluctuation as key excitations and established a multi-objective optimization model to minimize both the peak-to-peak transmission error and the fluctuation percentage of mesh stiffness. The Pareto-optimal solution set was obtained using the NSGA-II algorithm. Liu et al. [16] proposed a gear transmission optimization model based on dynamic fatigue reliability sensitivity. Zhang et al. [17] developed a digital twin-driven domain adaptation network for intelligent fault diagnosis of rolling bearings, effectively ascertaining the health status of critical components. Liu et al. [18] further contributed by presenting a systematic review of digital twin frameworks, emphasizing the integration of physical entities, virtual models, and twin data. Zhou et al. [19] proposed a vibration-based damage monitoring digital twin (VBDM-DT) for online intelligent assessment of wind turbine gearboxes. Validated on a 2 MW wind turbine, the approach provides credible and reliable remaining useful life predictions for gears and bearings. This model was used to identify the optimal structural parameters that minimize the system volume while satisfying dynamic fatigue reliability constraints, solved by a genetic algorithm.

The design of permanent magnet synchronous generators, which involves multiple interdisciplinary fields including electromagnetism, structural mechanics, and thermodynamics, has been extensively studied to achieve optimization objectives such as reduced cost, lower weight, higher efficiency, and vibration and noise suppression. Among them, Öztürk et al. [20] designed and optimized a surface-mounted PMSG for low-power wind turbines, focusing on the minimization of cogging torque ripple. Abdoos et al. [21] performed an optimal design of a radial-flux PMSG for direct-drive wind turbines, maintaining high system efficiency while reducing overall costs. A key feature of this study was the comprehensive accounting of all energy production costs, including the manufacturing of the generator, converter, electrical subsystem, and tower. Alemi-Rostami et al. [22] developed a stepwise design methodology for direct-drive PMSGs. The generator was modeled using the winding function method, its output characteristics were analytically calculated, and finally, designs with enhanced efficiency and power factor were identified through sensitivity analysis and genetic algorithm-based optimization. Jin et al. [23] investigated a novel annular winding PMSG, analyzing its no-load electromotive force and dynamic characteristics under different pole arc coefficients, and subsequently optimized this parameter. Emami et al. [24] considered multiple PMSG design parameters and conducted multi-objective optimization aimed at maximizing annual energy yield while minimizing torque ripple and losses. The proposed analytical model enabled the study of all possible pole-slot combinations, permanent magnet dimensions, and key stator geometries against a specific objective function. Mohd-Shafri et al. [25,26] established a finite element model for a three-phase, 12-slot/8-pole radially magnetized

PMSG. The motor design was optimized using a method combining a genetic algorithm with a sub-domain model to improve total harmonic distortion and cogging torque performance. Sindhya et al. [27] studied the analytical model of PMSGs and solved a mixed-constraint, multi-objective optimization problem with six objective functions using an interactive multi-objective optimization approach. Dang et al. [28, 29] proposed an optimization design method for a 10 MW offshore wind PMSG that considers its speed and torque distribution. Based on a d-q axis equivalent circuit model, this method can optimize time-varying control parameters with reduced computational time. Asef et al. [30] employed a dual-level response surface methodology to determine the optimal design parameters for maximizing the power output of an external-rotor surface-mounted PMSG. Additionally, using a simulated annealing algorithm, a design scheme for minimizing material cost under a constant volume constraint was identified. Jaen-Sola et al. [31] compared the performance of steel and composite material structures for a direct-drive PMSG under identical load conditions and proposed a lightweight structural design scheme.

In current design practice, gearboxes and generators are usually optimized separately. For gearboxes, many studies focus on volume reduction, lightweight design, power density improvement, and static reliability analysis. For permanent magnet synchronous generators (PMSG), research mainly aims at reducing cost, lowering weight, improving efficiency and suppressing vibration and noise. However, few studies treat the gearbox and generator as an integrated system for coupled parameter design. The independent design mode cannot achieve system-level optimal matching, making it difficult to meet the requirements of high power density and low dynamic load simultaneously.

To address the above problems, this work develops a two-level hierarchical mechatronic co-design framework for wind turbine gearbox–generator units. The proposed approach unifies static performance optimization and dynamic response refinement, and implements a progressive optimization pathway from global system matching to local component adjustment. This framework provides a new systematic method for developing high-performance wind turbine drivetrains.

2. Multi-level integrated design principles for gearbox-generator systems

The multi-stage integrated design method for the parameters of the wind turbine gearbox and generator comprises two distinct levels, as shown in **Figure 1**. The first stage concentrates on system-level static parameter matching to determine baseline electromechanical parameters via FEA and numerical iteration. Initial mechanical and electrical parameters are determined by combining numerical calculation and automated finite element analysis. Mechanical parameters (transmission ratio, speed, torque) are coupled with generator parameters through iterative adjustment. The optimization objectives are to maximize the overall power density of the gearbox–generator system and minimize the peak-to-peak values of internal excitations, including time-varying mesh stiffness and electromagnetic excitation ripples. To improve computational efficiency, shaft, bearing, and bolt connection stiffness are not considered in this stage, and FEA is automated through VB scripts.

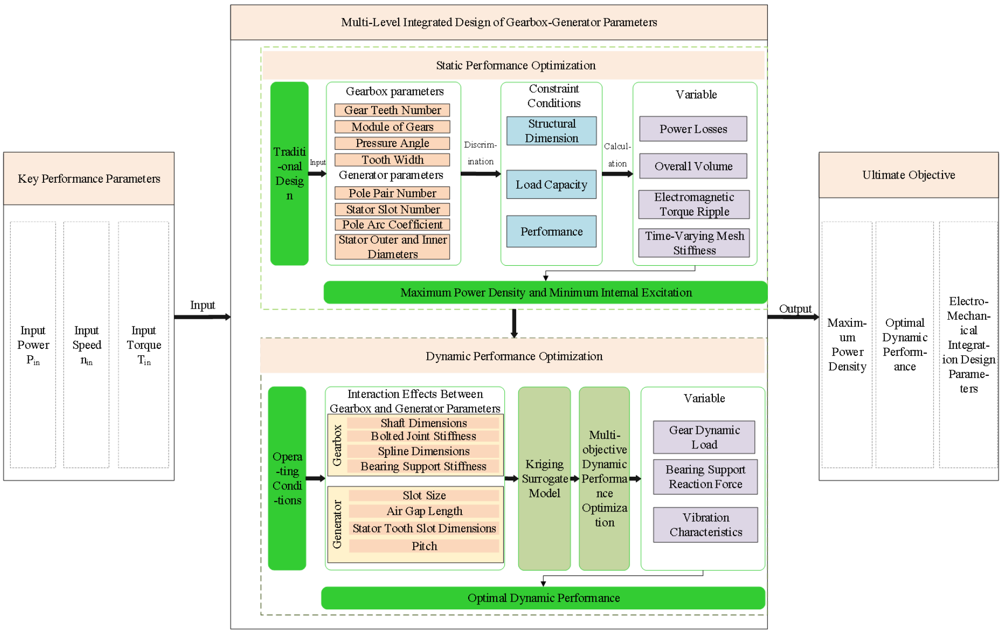

Figure 1. Flowchart of the multi-level integrated design process for wind turbine transmission system parameters.

Taking the results of Stage 1 as initial values, the second stage targets component-level dynamic refinement, where key structural parameters are optimized using a correlation-based surrogate model and a multi-objective algorithm. Key parameters include gearbox shaft dimensions, bearing stiffness, spline size, ring gear connection stiffness, and generator parameters such as air-gap length and slot opening size. Before optimization, correlation analysis is used to screen sensitive parameters that significantly affect dynamic responses, thus reducing the optimization dimension. A Kriging meta-model is then established to capture the nonlinear mapping between electromechanical parameters and dynamic responses. Finally, the NSGA-II multi-objective optimization algorithm is used to obtain the optimal parameter set with excellent dynamic performance.

The detailed electromechanical coupling dynamic model of the wind turbine gearbox-generator system has been established in previous work [32]. Here, we summarize the core equations that govern the coupling between the mechanical drivetrain and the electrical generator, which are used to compute the dynamic responses in the subsequent optimization.

Mechanical subsystem: The gearbox is modeled as a translational-torsional lumped-parameter system. The meshing element mainly includes the sun-planet and planet-ring meshing elements. The dynamic model of the planetary gear system was constructed using the rotating coordinate system of the planetary carrier rotation. The translation–torsion dynamic model of the planetary gear mechanism is shown in **Figure 2**. The dynamic meshing force and time-varying meshing stiffness of the gear are calculated by Equation (1):

$$\begin{cases} F_m(t) = k_m(t)\delta(t) + c_m\dot{\delta}(t) \\ k_m(t) = \bar{k}_{spn} + \sum_{t=1}^{20} k_{spnt}cos(\frac{t\pi r_{pn}\theta_{pn}}{\frac{w_{pn}p_{bt}}{2}} + \nu_{spn}) \end{cases}, \tag{1}$$

where $k_m(t)$ is the time-varying mesh stiffness, c_m the mesh damping, and $\delta(t)$ is the dynamic transmission error. The stiffness $k_m(t)$ is calculated using the energy method as detailed in Chen et al. [32].

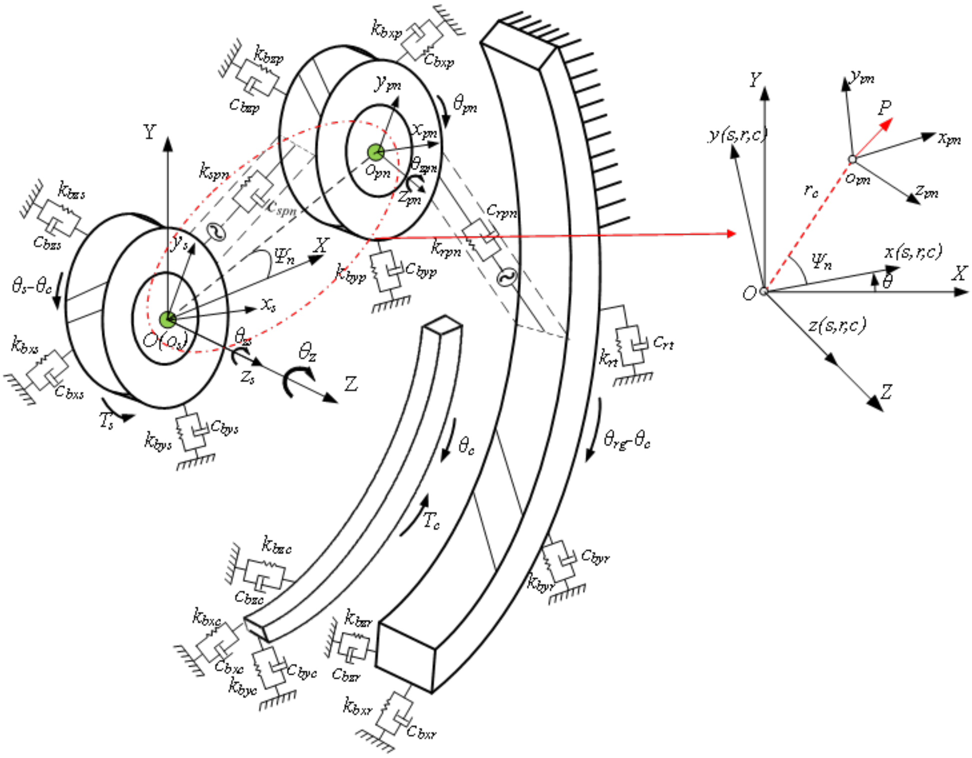

Figure 2. Translation-torsion dynamic model of the planetary gear system.

As shown in **Figure 2**, the direction from the sun gear to the planetary gear is set as the positive direction of the meshing line, and the direction from the planetary gear to the inner ring gear is set as the positive direction of the meshing line. The meshing deformations of the inner and outer gears of the planetary gear system δ_{rpi} and δ_{spi} can be obtained as follows:

$$\begin{cases} \delta_{rpn} = [(y_r - y_{pn})\cos(\varphi_{rn}) + (-x_r + x_{pn})\sin(\varphi_{rn}) \\ \quad + r_r(\theta_r - \theta_c) - r_p\theta_{pn}]\cos\beta + (z_r - z_{pn})\sin\beta + e_{rpn}(t) \\ \delta_{spn} = [(y_s - y_{pn})\cos(\varphi_{sn}) + (x_s - x_{pn})\sin(\varphi_{sn}) \\ \quad + r_s(\theta_s - \theta_c) + r_p\theta_{pn}]\cos\beta + (-z_s + z_{pn})\sin\beta + e_{spn}(t) \end{cases}, \tag{2}$$

where α_{rp} and α_{sp} are the internal and external meshing pressure angles, respectively; r_r, r_s, and r_p are the radii of the base circle of the ring gear, sun gear, and planetary gear, respectively; and φ_{rn} and φ_{sn} can be expressed as $\varphi_{rn} = \psi_n + \alpha_{rp}$ and $\varphi_{sn} = \psi_n - \alpha_{sp}$, respectively.

Electrical subsystem (PMSG): The permanent magnet synchronous generator is described by a nonlinear d-q axis model accounting for magnetic saturation and spatial harmonics. The variables in the Equations (3) are computed via finite element software based on the actual generator structure.

$$\begin{cases} U_d = R\, i_d + [L_d(i_d, i_q\quad)\frac{\mathrm{d}i_d}{\mathrm{d}t} + i_d\frac{\mathrm{d}L_d(i_d,i_q)}{\mathrm{d}t} + \frac{\mathrm{d}\varphi_1(i_d,i_q)}{\mathrm{d}t}\quad] - \omega_\mathrm{r} L_q\left(i_d, i_q\right) i_q + \sum_{k=1}^{\Lambda}\sum_{h=1}^{\Omega} \varphi_{dft}\omega_r \sin f_t, \\ U_q = R\, i_q + \left[L_q\left(i_d, i_q\right)\frac{\mathrm{d}i_q}{\mathrm{d}t} + i_q\frac{\mathrm{d}L_q(i_d,i_q)}{\mathrm{d}t}\right] + \omega_\mathrm{r} L_d\left(i_d, i_q\right) i_d + \omega_r\varphi_1\left(i_d, i_q\right) + \sum_{k=1}^{\Lambda}\sum_{h=1}^{\Omega} \varphi_{qft}\omega_\mathrm{r} \sin f_t, \\ T_\mathrm{e} = \frac{3p_\mathrm{n}}{2}\left\{\varphi_1\left(i_d, i_q\right) i_q + \left[L_d\left(i_d, i_q\right) - L_q\left(i_d, i_q\right)\right] i_d i_q + \sum_{k=1}^{\Lambda}\sum_{h=1}^{\Omega} \varphi_{dft} i_d \sin f_t + \sum_{k=1}^{\Lambda}\sum_{h=1}^{\Omega} \varphi_{qft} i_q \sin f_t\right\}, \\ F_\mathrm{r}(\theta, t) = \frac{1}{2\mu}\left(B_\mathrm{r}^2(\theta, t) - B_\mathrm{t}^2(\theta, t)\right), \\ F_\mathrm{t}(\theta, t) = \frac{1}{2\mu} B_\mathrm{r}(\theta, t) B_\mathrm{t}(\theta, t). \end{cases} \tag{3}$$

where U_d and U_q are the d- and q-axis voltages, i_d and i_q are the d- and q-axis currents, ω_{ro} is the generator rotor speed, R is phase resistance, T_e is the electromagnetic torque, f_t is the harmonic frequency of the electromagnetic excitation frequency, and f_e is the electromagnetic excitation frequency.

The electromechanical coupling dynamic model of the wind turbine drivetrain is established by integrating the dynamic submodels of each component and the internal/external excitation models. From an energy perspective, the energy conversion process in the generator occurs via the air-gap magnetic field as the coupling field, sequentially converting mechanical energy into magnetic energy and then into electrical energy. By establishing the linkage between the mechanical and electrical systems, an electromechanical-rigid-flexible coupling dynamic model of the integrated gearbox-generator transmission system is obtained, as given in Equation (4).

Numerical simulation models of the three-phase permanent magnet synchronous generator (PMSG) and the multistage gear system are separately constructed using numerical computation software. Combined with the vector control method, the generator torque and rotational speed are used as real-time coupling variables between the gear system and the generator. Specifically, the electromagnetic torque and the rotor speed serve as common variables that are transferred between the two subsystems in real time. The model is solved in the MATLAB/Simulink environment using the built-in ode45 solver (a fourth-order/fifth-order Runge-Kutta algorithm).

$$\begin{cases} \begin{pmatrix} M_a + M_{sa}(X) & 0 \\ 0 & M_c \end{pmatrix}\begin{pmatrix} \ddot{X}_a \\ \ddot{X}_c \end{pmatrix} + \begin{pmatrix} C_a + C_{sa}(X) + C_m(X) & 0 \\ 0 & C_h \end{pmatrix}\begin{pmatrix} \dot{X}_a \\ \dot{X}_h \end{pmatrix} \\ + \begin{pmatrix} K_a + K_{sa}(X) + K_m(X) + K_{\mathrm{be}11} & -K_{\mathrm{be}12} \\ -K_{\mathrm{be}21} & K_h + K_{\mathrm{be}22} \end{pmatrix}\begin{pmatrix} X_a \\ X_h \end{pmatrix} = F(t) + F_{sa}(X_a), \\ U = RI + \frac{d\psi}{dt} = RI + L\frac{dI}{dt} + \frac{dL}{d\theta_{ro}}\omega_r I, \\ F_r(\theta, t) = \frac{1}{2\mu}(B_r^2(\theta, t) - B_t^2(\theta, t)), \\ F_t(\theta, t) = \frac{1}{2\mu} B_r(\theta, t) B_t(\theta, t), \\ T_\mathrm{in} = \frac{1}{2}\rho\pi R_{tur}^5\left(\frac{1}{\lambda_{opt}}\right)^3 C_p w_{tur}^2, \\ T_e = \frac{3n_p}{2}\{\varphi_r(i_d, i_q) i_q + [L_d(i_d, i_q) - L_q(i_d, i_q)] i_d i_q + \ldots\}. \end{cases} \tag{4}$$

3. Static-performance-driven integrated design

3.1. First-level parameter integration

In this study, a multi-objective optimization framework is developed for the integrated gear-train and generator design of direct-drive wind turbines. As shown in **Figure 3**, the initial gear and generator parameters are determined via physics-based numerical models incorporating torque-speed relationships, power density constraints, and material fatigue limits. To minimize computational cost, generator performance is evaluated only after the gear parameters satisfy all mechanical constraints, as finite element analysis (FEA) of the generator is computationally intensive. Annual wind speed data measured at 120 m height are used to determine the turbine' s turbine' s optimal operating speed, thereby deriving the corresponding torque and power input to the gear transmission. NSGA-II is employed to optimize the following gear design variables: sun and planet gear tooth counts, face width, module, and pressure angle. Following constraint satisfaction, the following performance metrics are computed: friction loss, transmission efficiency, system volume, and time-varying mesh stiffness. The transmission ratio, generator rotational speed, and output torque are computed based on the optimized gear geometry. Standard electromagnetic design methods are applied to determine pole pairs, stator slot count, rotor diameter, and core length. A spatial constraint is imposed such that the stator outer diameter must not exceed the inner diameter of the high-speed-stage internal gear ring. Generator parameters are imported into FEA scripts for verification. If all constraints are satisfied, electromagnetic torque, radial force, output power, and iron loss are extracted; otherwise, the generator design variables are adjusted and re-optimized. The multi-objective optimization aims to maximize power density and minimize the peak-to-peak amplitudes of: (1) time-varying mesh stiffness, (2) electromagnetic torque ripple, and (3) electromagnetic radial force ripple. Following convergence, the Pareto-optimal front is generated. A final design is selected based on a weighted trade-off between power density, vibration suppression, and manufacturability.

3.2. Integrated optimization model and variable selection

Wind turbine drivetrain design is a typical multi-objective optimization problem with conflicting objectives. In this paper, the NSGA-II algorithm is adopted to obtain a well-distributed Pareto front.

Design variables include key geometric parameters of the three-stage planetary gear system and the PMSG. For the gear system, variables include tooth numbers, module, and face width of sun and planet gears. For the generator, variables include stator outer/inner diameter, air-gap length, pole arc coefficient, permanent magnet dimensions, slot width, core length, and phase current. Consequently, these parameters, along with key coefficients from their governing equations, are selected as the primary design variables. Detailed variable and value ranges are listed in **Table 1**.

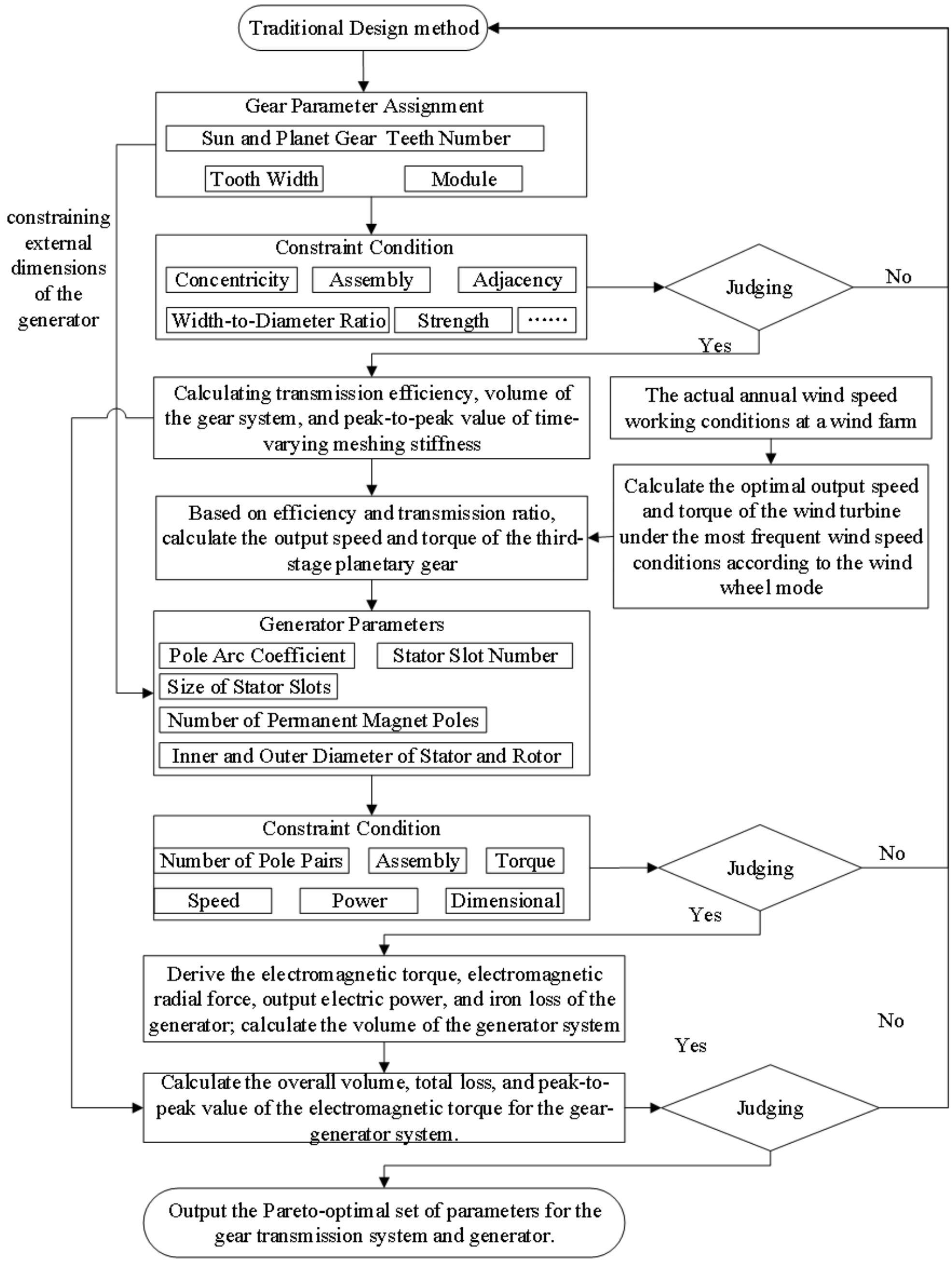

Figure 3. First-level integrated design of gearbox-generator parameters.

Table 1. Gear and generator system design parameter.

Optimization variables		**Indexing**	**Optimization range**
Low-speed planet gear system	Tooth number of sun gear Z_{s1}	x_1	[17, 65]
	Tooth number of planet gear Z_{p1}	x_2	[17, 45]
	Modulus m_{n1}	x_3	First and Second Series
	Gear width b_{11}	x_{10}	[0.25, 0.75]
Medium-speed planet gear system	Tooth number of sun gear Z_{s2}	x_4	[17, 65]
	Tooth number of planet gear Z_{p2}	x_5	[17, 45]
	Modulus m_{n2}	x_6	First and Second Series
	Gear width b_{22}	x_{11}	[0.15, 0.60]
High-speed planet gear system	Tooth number of sun gear Z_{s3}	x_7	[17, 65]
	Tooth number of planet gear Z_{p3}	x_8	[17, 60]
	Modulus m_{n3}	x_9	First and Second Series
	Gear width b_{33}	x_{12}	[0.08, 0.4]

Table 1. *Cont.*

Optimization variables		Indexing	Optimization range
Generator system	Stator outer diameter D_{so}/mm	x_{13}	[1,000, 3,000]
	Air gap length *Gap*/mm	x_{14}	[1, 16]
	Pole Arc Coefficient α	x_{15}	[0.5, 0.9]
	Electrical frequency f_e/Hz	x_{16}	[50, 100]
	Number of slots per phase per pole q	x_{17}	[1, 8]
	Thickness of the permanent magnet W_t/mm	x_{18}	[5, 40]
	Width of the permanent magnet, W_m/mm	x_{19}	[17, 65]
	Pitch	x_{20}	[1, 15]
	Width of the stator slot S_{w1}/mm	x_{21}	[8, 35]
	Height of the stator slot S_{w4}/mm	x_{22}	[40, 120]
	Core length H/mm	x_{23}	[300, 1,200]
	Stator phase current I_a/A	x_{24}	[6,000,12,000]

$$[x_1, x_2, x_3, x_4, x_5, x_6, x_7, x_8, x_9, x_{10}, x_{11}, x_{12}, x_{13}, x_{14}, x_{15}, x_{16}, x_{17}, x_{18}, x_{19}, x_{20}, x_{21}, x_{22}, x_{23}, x_{24}] = [z_{s1}, z_{p1}, m_{n1}, z_{s2}, z_{p2}, m_{n2}, z_{s2}, z_{p2}, m_{n3}, b_{11}, b_{22}, b_{33}, D_{so}, Gap, \alpha, f_e, q, W_t, W_m, Pitch, S_{w1}, S_{w4}, H, I_a]. \quad (5)$$

Where, z_{s1} and z_{p1} denote the tooth numbers of the sun and planet gears in the low-speed stage, with m_{n1} and b_{11} being their module and face width; z_{s2} and z_{p2} represent those for the medium-speed stage, with m_{n2} and b_{22} as the corresponding module and face width; and z_{s3}, z_{p3}, m_{n3}, b_{33} are the analogous parameters for the high-speed stage. As illustrated in **Figure 4**, D_{so} and D_{si} denote the outer and inner diameters of the stator, respectively, and H represents the stack length. S_{w4} refers to the yoke width of the stator core, while S_{w1} and S_{w2} designate the stator slot width and slot opening width, respectively. *Gap* is the air gap length, S_T the slot depth, and W_t and W_m the thickness and width of the permanent magnet. D_{ro} and D_{ri} indicate the outer and inner diameters of the rotor.

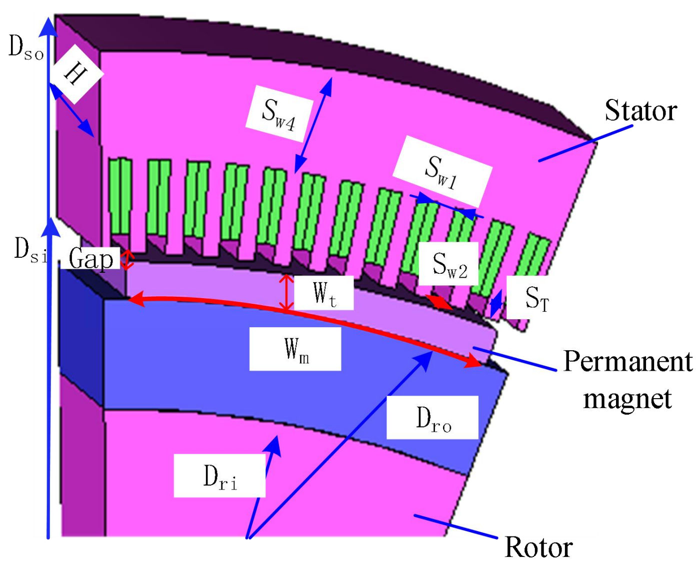

Figure 4. Structural parameters of the permanent magnet generator.

3.3. Optimization objectives for the integrated system

The annual average wind speed of the target wind farm is 7.8 m/s, and the wind turbine operates in the range of 4–20 m/s. Since rated operating conditions (10–20 m/s) last the longest, optimization is mainly carried out based on rated conditions. The core optimization objectives are:

1. Maximize the volumetric power density of the gearbox–generator system.
2. Minimize the peak-to-peak values of time-varying mesh stiffness for all gear stages.
3. Minimize the peak-to-peak values of electromagnetic torque ripple and electromagnetic radial force ripple.

Power density is defined as the ratio of net output power to total system volume, considering gear meshing loss, bearing loss, generator iron loss, copper loss, and stray loss.

$$\begin{aligned} F(x) &= 0.4 \times max(P_1) + 0.1 \times min(k_{m1\_peak}) + 0.1 \times min(k_{m2\_peak}) \\ &+0.1 \times min(k_{m3\_peak}) + 0.15 \times min(T_{e\_peak}) + 0.15 \times min(F_{r\_peak}). \end{aligned} \tag{6}$$

Where *F(x)* represents the optimization objective function, P_1 represents the power density of the system, k_{m1_peak}, k_{m2_peak} and k_{m3_peak} represent peak-to-peak time-varying mesh stiffness of gear systems, T_{e_peak} represent peak-to-peak electromagnetic torque, F_{r_peak} represent peak-to-peak electromagnetic radial force (**Figure 5**).

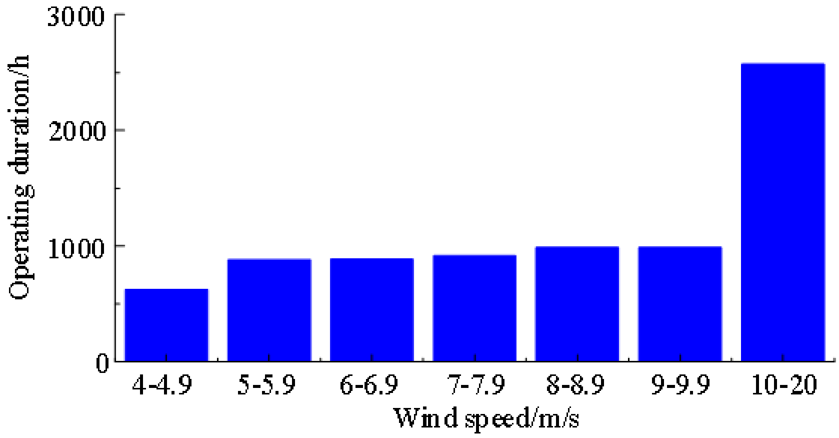

Figure 5. Annual wind speed condition of a wind farm.

Integrated system optimization design objective—Power density

In traditional optimization designs, the volume or mass of the wind turbine drivetrain system is used as the optimization objective, but this can result in sacrificing some power, making the optimization process limited. Therefore, this paper adopts the overall power density of the wind turbine drivetrain as the optimization objective. The system output power P_{out} refers to the rated output power of the generator. Based on these volume and power definitions, the overall system power density is formulated as:

$$\begin{cases} P_1 = \dfrac{P_{out}}{V} \\ \text{V=}\sum_{i=1}^{3} V_{mi} + V_g \\ V_{mi} = \left(\dfrac{m_{ni}z_{si}}{2}\right)^2 b_{si} + \left(\dfrac{m_{ni}z_{pi}}{2}\right)^2 b_{pi}n_{pi} + \left(\dfrac{D_{nfi}+B_i}{2}\right)^2 b_{ni} \\ B_i = -\left(3\left(D_{nfi}-D_{bni}\right) - \dfrac{b_{ni}[\sigma]}{F_{ti}\times 10^6}\right) + \sqrt{\left(3\left(D_{fni}-D_{bni}\right) - \dfrac{b_{ni}[\sigma]}{F_{ti}\times 10^6}\right)^2 - 12b_{ni}} \\ V_g = V_s + V_{ro} + V_p \\ V_s = \dfrac{H\pi((D_{so}^2 - D_{si}^2)}{4} - S_{w1} * Slots(\dfrac{D_{so}-D_{si}}{2} - S_{w4})) \\ V_{ro} = \pi H \dfrac{(D_{ro}^2 - D_{ri}^2)}{4} \\ V_p = HW_tW_m. \end{cases} \tag{7}$$

Here, V_{mi} denotes the volume of the i-th stage gear system volume, (with i = 1, 2, 3 corresponding to the low-, medium-, and high-speed stages, respectively), This includes design parameters such as the number of planet gears n_{pi}, the root circle diameter D_{nfi} and thickness B_i of the ring gear, $[\sigma]$ represents the allowable stress of the gear material, D_{bni} represents the pitch circle diameter of the ring gear. The generator volume V_g consists of the stator volume V_s and the generator rotor volume.

The operation of a wind turbine generator involves the conversion of wind energy into mechanical energy, which is subsequently transformed into electrical energy, with inherent energy losses occurring throughout this process. This study focuses on the following loss types: gear meshing losses, bearing losses, as well as generator iron losses, copper losses, and mechanical losses. The actual output power of the wind turbine drive system needs to consider the actual losses in the gear system and the generator system. This can be expressed as follows:

$$\begin{cases} P_{\text{in}} = \dfrac{\pi}{2} C_p \rho R^2 v^3 \\ P_{\text{out}} = P_{\text{in}} - P_{gloss} - P_{\text{in}}\eta_m\eta_n \end{cases}. \tag{8}$$

Within the gear system, the main losses include those from gear meshing, bearings, and oil churning. Among these, the power loss due to gear meshing constitutes the dominant portion of the total power loss in the gear transmission system. The gear meshing efficiency loss can be expressed by Equation (9):

$$\begin{cases} \eta_m = 1 - \mu_{mz}H_v \\ H_v = \dfrac{(i \pm 1)\pi}{z_1 icos(\beta)}(1 - \varepsilon_a + \varepsilon_1^2 + \varepsilon_2^2) \\ \varepsilon_a = \dfrac{1}{2\pi}[z_1(tan\alpha_{at1} - tan\alpha_t^{'}) \pm z_2(tan\alpha_{at2} - tan\alpha_t^{'})] \\ \varepsilon_1 = \dfrac{z_1}{2\pi}\left|tan\alpha_{at1} - tan\alpha_t^{'}\right| \\ \varepsilon_2 = \dfrac{z_2}{2\pi}\left|tan\alpha_{at2} - tan\alpha_t^{'}\right|. \end{cases} \tag{9}$$

Where μ_{mz} represent average coefficient of friction during meshing, generally takes a value between 0.06 and 0.10. H_v represent power loss factor. For external meshing, take '+', for internal meshing, take '−', i is the gear ratio, z_1 is the number of teeth on the driving gear, β is the helix angle, ε_a is the total face contact ratio, ε_1 is the face contact ratio at entry, and ε_2 is the face contact ratio at exit. α_{at1} represent addendum circle pressure angle, $\alpha_t^{'}$ represent meshing angle.

When the number of planet gears is equal to or greater than three, only bearing losses of the planet gears are considered, and the bearing efficiency η_n can be calculated using the bearing loss coefficient ψ_n.

$$\begin{cases} \eta_n = 1 - \dfrac{i_{rs}}{i_{rs}+1}\psi_n,\ i_{rs} = \dfrac{z_r}{z_s} \\ \psi_n = \dfrac{\sum_{i=1}^{k} T_{ni} n_i}{T_s n_s},\ T_n = \dfrac{0.5\mu F d}{1000} \end{cases} . \tag{10}$$

Where T_{ni} represents the friction torque of the bearing, n_i is the rotational speed of the bearing, T_s is the output shaft torque, n_s is the rotational speed of the output shaft, k is the number of planet gear bearings; μ is the bearing friction coefficient (in this article, μ is taken as 0.0011); F is the load acting on the bearing, d is the inner diameter of the bearing.

The main losses in the generator consist of iron losses P_{ir}, stator armature losses P_{cu}, and stray losses P_{stray}, as given in Equation (11). Iron losses induced by time-varying magnetic flux density can be classified into three components: hysteresis loss, eddy current loss, and excess loss. In this study, excess loss is incorporated into the stray loss category. Core loss calculation is performed using the finite element method, accounting for the nonlinear magnetic saturation behavior of the core material. Stray losses, also referred to as mechanical losses, are estimated at 3% of the total mechanical power input to the generator.

$$\begin{cases} P_{\text{gloss}} = P_{cu} + P_{ir} + P_{stray} \\ P_{ir} = (P_{et} + P_{ht})V_t + (P_{ey} + P_{hy})V_y \\ P_{et} = \dfrac{4m}{\pi^2} q k_q k_l k_e (w_r B_t)^2 \\ P_{ey} = \dfrac{8}{\alpha\pi^2} q k_e k_\gamma (w_r B_e)^2 \\ P_{ht} = k_h w_r B_t^{\beta} \\ P_{hy} = k_h w_r B_e^{\beta} \\ B_e = \dfrac{\sqrt{2} p U_e}{\pi w_r r_s H N k_a}, B_t = (1-\lambda_s)B_e,\ B_d = \dfrac{r_s \pi}{2 p d_b} B_e \\ P_{cu} = 3 R_a I_a^2 \\ R_a = N_{slot} N \rho (2H + \pi W_s) \\ P_{\text{stray}} = 3\% T_{ro} w_{ro}. \end{cases} \tag{11}$$

Where V_t and V_y denote the total volumes of the stator teeth and stator yoke, respectively. The corresponding unit-volume losses are expressed by P_{et} and P_{ht} for the eddy current and hysteresis losses in the stator teeth, and P_{ey} and P_{hy} for those in the stator yoke. The electromagnetic and structural parameters include: the number of phases, m; k_e represents the eddy current coefficient; k_q represents the correction coefficient related to electrical symmetry; k_l represents the motor correction coefficient; q represents the number of slots per pole per phase; k_h represents the hysteresis coefficient; β is the Steinmetz coefficient, determined by the material. air gap magnetic density B_e, the stator tooth magnetic density B_t, and the stator yoke magnetic density B_d, p represents the number of pole pairs of the generator; U_e represents the air-gap voltage; w_r represents the angular velocity of the rotor; r_s represents the inner diameter of the stator; N represents the number of turns in the coil. λ_s represents the short pitch coefficient; d_b represents the width of the stator yoke. ρ represents resistivity of the winding, N_{slot} represents generator slot count.

The main parameters affecting the dynamic performance of the system are the peak-to-peak values of the generator's electromagnetic torque fluctuation, electromagnetic radial force fluctuation, and the time-varying meshing stiffness peak-to-peak values of the gear system. The electromechanical coupling dynamics model can be seen in Chen et al. [32]. For calculating the electromagnetic torque of a permanent magnet synchronous generator (PMSG), it is known that the electromagnetic torque of a PMSG is derived from the d-axis and q-axis currents and the flux linkage. Since the flux linkage is a function of the currents, controlling the d-axis and q-axis currents can achieve torque tracking. Through the methods described in Chen et al. [32]. For calculating electromagnetic torque and electromagnetic radial force, the peak-to-peak values of electromagnetic torque and electromagnetic radial force can be obtained. The peak-to-peak values of time-varying meshing stiffness in the gear system are calculated using the energy method, which can refer to the calculation formula for time-varying meshing stiffness in the internal excitation model of the gear system presented in Chen et al. [32].

$$\begin{cases} \mathrm{T}_{\mathrm{e}_{\_peak}} = \mathrm{T}_{\mathrm{e}_{\_\max}} - \mathrm{T}_{\mathrm{e}_{\_\min}} \\ k_{\mathrm{sp1}_{\_peak}} = k_{\mathrm{sp1}_{\_\max}} - k_{\mathrm{sp1}_{\_\min}} \\ k_{\mathrm{sp2}_{\_peak}} = k_{\mathrm{sp2}_{\_\max}} - k_{\mathrm{sp2}_{\_\min}} \\ k_{\mathrm{sp3}_{\_peak}} = k_{\mathrm{sp3}_{\_\max}} - k_{\mathrm{sp3}_{\_\min}} \\ F_{\mathrm{r}_{\_peak}} = F_{\mathrm{r}_{\_\max}} - F_{\mathrm{r}_{\_\min}} \end{cases}. \tag{12}$$

3.4. Design constraints for integrated system parameters

The design constraints for the wind turbine gearbox–generator drivetrain system are categorized into two groups: those imposed on the basic parameters of the gear system and those applied to the structural parameters of the generator. The constraints related to the gear system are further divided into structural assembly constraints and static strength constraints. Structural assembly constraints include concentricity, assemblablity, and adjacency conditions, while static strength constraints encompass the diameter-to-width ratio, bending fatigue strength at the tooth root, and surface contact fatigue strength. The constraint equations are as follows:

$$\begin{cases} \dfrac{z_s+z_p}{cos(\alpha_{sp})}-\dfrac{z_r-z_p}{cos(\alpha_{rp})}=0 \\ \dfrac{z_{s1}+z_{r1}}{n}=\text{Integer number} \\ z_p+2(h_a^*+x_p)-(z_s+z_p)*sin(\dfrac{\pi}{n})\leq 0 \\ 0.4m_t-S_{ai}\leq 0 \\ \alpha_t-\dfrac{n(h_a^*-x_s)}{z_s sin2\alpha_t}-tan\alpha_{sp}+\dfrac{z_p}{z_s}(tan\alpha_{ap}-tan\alpha_{sp})\leq 0 \\ z_r(inv\alpha_{ar}+\delta_r)-z_p(inv\alpha_{ap}+\delta_p)-(z_r-z_p)inv\alpha_{rp}\leq 0 \\ \dfrac{z_r}{z_p}\left[arcsin\sqrt{\dfrac{(\left(\frac{cos\alpha_{ar}}{cos\alpha_{ap}}\right)^2-1)}{(\left(\frac{z_r}{z_p}\right)^2-1)}}+inv\alpha_{ar}-inv\alpha_{rp}\right] \\ -\left[arcsin\sqrt{\dfrac{(1-\left(\frac{cos\alpha_{ap}}{cos\alpha_{ar}}\right)^2)}{(1-\left(\frac{z_p}{z_r}\right)^2)}}+inv\alpha_{ap}-inv\alpha_{rp}\right]\leq 0 \end{cases} \tag{13}$$

Where S_{ai} represents the tooth tip thickness of the sun gear, planet gear, and ring gear. α_t represents pitch circle pressure angle of sun and planet gear, α_{as}, α_{ap}, α_{ar} represents addendum circle pressure angle of sun, planet gear, and ring gear.

The primary input variables for the permanent magnet generator design include the rated power range, rated frequency, line voltage, and number of phases. Based on these inputs, key operational parameters such as the rated speed, torque, and number of pole pairs are derived using relevant analytical formulations. The main dimensions of the generator—specifically, the stator inner diameter and the effective core length—are determined with consideration to both economic feasibility and operational rationality, as these dimensions directly influence generator performance metrics such as efficiency and power factor (**Table 2**).

Table 2. Generator system basic parameter range.

	Names	Symbols	Value of number
Design Input Variables	Line Voltage	$U_{L\text{-}L}$	1,200 V
	Rated Power	P_N	8.25~8.6 MW
	Tooth Flux Density of Stator	B_t	1.1~2.2 T
	Yoke Flux Density of Stator	B_d	1.1~2.2 T
	Slots per Pole per Phase	q	2~5
Design Assumption Parameters	Generator Line Load	A	200~650 A/cm
	Current Density	J_s	3~4.7 A/mm^2
	Utilization Factor of Permanent Magnets	c_v	0.4~0.6
	Coercivity of Permanent Magnets	H_c	7 × 10^5 AT/m
	Remanent Flux Density	B_r	0.8~1.2 T
	Maximum Air Gap Flux Density	B_g	0.7~0.9 T

The performance of a permanent magnet generator is largely determined by basic parameters such as pole pair number, phase current, and stator slot count, with the air gap length being especially critical. The governing relationship for the air gap is provided in Equation (14).

$$\begin{cases} 2p_n = \dfrac{120f_e}{n_N},\ Slots = 2p_n mq \\ I_N = \dfrac{P_N * 10^{-3}}{\sqrt{3}U_N cos\varphi} \\ 1 \le Gap \le 16 \end{cases} . \tag{14}$$

Where p_n represents number of pole pairs, I_N represents RMS phase current, U_N represents RMS phase voltage, $Slots$ represents number of stator slots.

The basic structural dimensions of a permanent magnet generator, such as the stator inner diameter, rotor outer diameter, and permanent magnet geometry, can be determined from empirical formulas. A key design consideration is the permanent magnet volume, which is a function of the air-gap power and the magnet material. Consequently, the careful selection of the magnet's width and length is essential, as expressed in Equation (15):

$$\begin{cases} D_{si} = \sqrt{\dfrac{6.1P_N}{\alpha_p K_B K_{w1} A B_g n_N H}} \\ D_{ro} = D_{si} - 2GAP - 2W_t,\ D_{ri} = (0.5 \sim 0.85) * D_{ro} \\ N = \dfrac{A\pi D_{\text{ro}}}{mI_N},\ N_s = \dfrac{Nma}{Z} \\ \tau = \pi D_{\text{si}}/2p_n \\ V_{gm} = c_v \dfrac{P_{ag}}{B_r H f_e} \\ w_{m1} = \dfrac{gB_g k_{sat}}{\mu_0 H(1 - \frac{B_g}{B_r}k_{sat}), w_{m2} = \frac{a_c k_1 k_j D\pi}{2pH}} \\ w_t = \dfrac{gB_g}{B_r - B_g}, \dfrac{w_m}{w_t} \le 15 \end{cases} . \tag{15}$$

Where N represents the number of conductors in series per phase, N_s represents the number of conductors per slot, a_p represents the number of parallel paths, Z represents the number of stator slots, c_v represents the utilization factor of permanent magnets, k_{sat} represents the saturation factor, k_j represents the distribution factor, w_{m1} and w_{m2} represent the minimum and maximum widths of permanent magnets, α represents the pole arc coefficient, K_B represents the waveform factor of the magnetic field, K_{w1} represents the armature fundamental winding factor, A represents the generator line load, B_g represents the maximum air gap flux density, n_N represents the generator rotor speed.

3.5. Analysis and results of the integrated optimization

The NSGA-II algorithm is used with a population size of 32 and maximum iterations of 90, converging after 1,680 effective evaluations. **Figure 6** shows the resulting Pareto front, visualized in terms of power density, peak-to-peak electromagnetic torque, and peak-to-peak time-varying meshing stiffness of the high-speed stage. To validate the feasibility of the optimization outcomes, three design schemes were selected from the Pareto front, as summarized in **Table 3**. The corresponding transmission ratios for these schemes are 78.36, 67.53, and 125.44, respectively. Three design schemes are selected for comparison, as listed in **Table 3**.

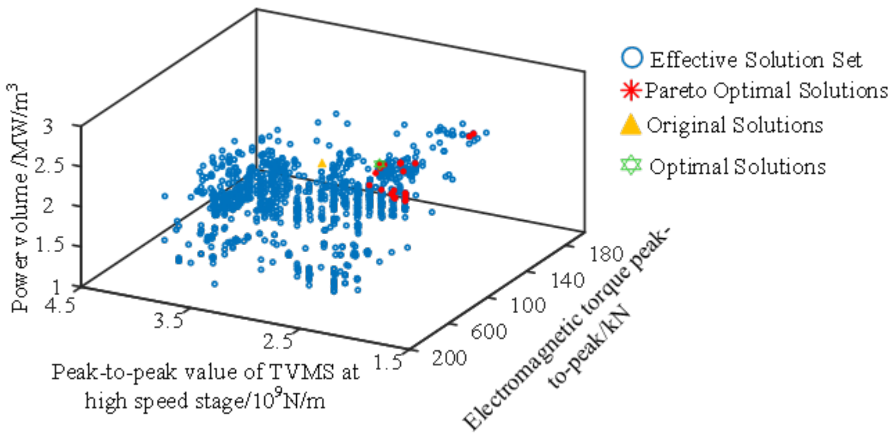

Figure 6. Pareto frontier solution.

Table 3. The optimized design scheme.

		Initial design	**Optimized design one**	**Optimized design two**	**Optimized design three**
Low-speed Gear system	Number of tooth	47/31/107	44/40/124	55/43/141	41/43/127
	Modulus/mm	24	20	20	21
	Tooth width/mm	490	380	378	420
	Number of planet gear	7	5	5	5
Medium -speed Gear system	Number of tooth	27/31/89	19/33/85	42/34/110	25/45/115
	Modulus/mm	23	18	20	20
	Tooth width/mm	350	280	300	295
	Number of planet gear	4	4	4	4
High-speed Gear system	Number of tooth	34/43/122	56/49/154	18/30/78	30/54/138
	Modulus/mm	13	9	14	11
	Tooth width/mm	230	180	240	200
	Number of planet gear	3	3	3	3
Permanent magnet generator	Pair of poles	8	8	8	4
	Number of tooth space	192	192	192	96
	Electrical frequency /Hz	100	125	100	100
	Stator inside and outside diameter /mm	1,830/2,160	1,663/1,995	1,930/2,002	1,630/2,120
	Slot width /mm	14	19	13	26.7
	Permanent magnet width and length /mm	30/312.3	16/368	15/256.6	25/303
	Gap length /mm	6	8.5	5	4
	Pitch	10	9	12	9
	Core length /mm	570	375	843	469
	Phase current /A	9,762.5	1,150	11,000	8,500
	Rated speed /r/min	700	850	680	1,400

Figure 7 compares the three design schemes in terms of power density, peak-to-peak electromagnetic torque fluctuation, and peak-to-peak time-varying meshing stiffness. Compared to the original design, Optimization Scheme One achieves a 35% improvement in power density. The peak-to-peak electromagnetic torque and electromagnetic radial force are reduced by 54% and 47%, respectively, while the peak-to-peak time-varying meshing stiffness decreases by 43%, 57%, and 32% for the low-, medium-, and high-speed stage external meshing, respectively.

Optimization Scheme Two yields a modest 2% increase in power density. It achieves greater reductions in electromagnetic torque fluctuation (62%) and moderate improvements in radial force (33%). The reductions in time-varying meshing stiffness are 47%, 48%, and 34% across the three stages. Optimization Scheme Three shows a 27% gain in power density, along with the highest reduction in electromagnetic torque fluctuation (63.9%) and a 50% decrease in radial force. The reductions in time-varying meshing stiffness are 45%, 34%, and 4% for the three stages. Further analysis reveals that gear meshing losses can be reduced by decreasing and balancing the engagement and exit overlap ratios. For the generator, higher rotational speeds lead to a more compact size, longer core length, and lower flux density, thereby reducing iron losses. It should be noted that higher-speed designs may require enhanced cooling and rotor retention, which are not modeled in this study. Based on a comprehensive evaluation of all performance metrics, optimization scheme one is selected as the optimal integrated design.

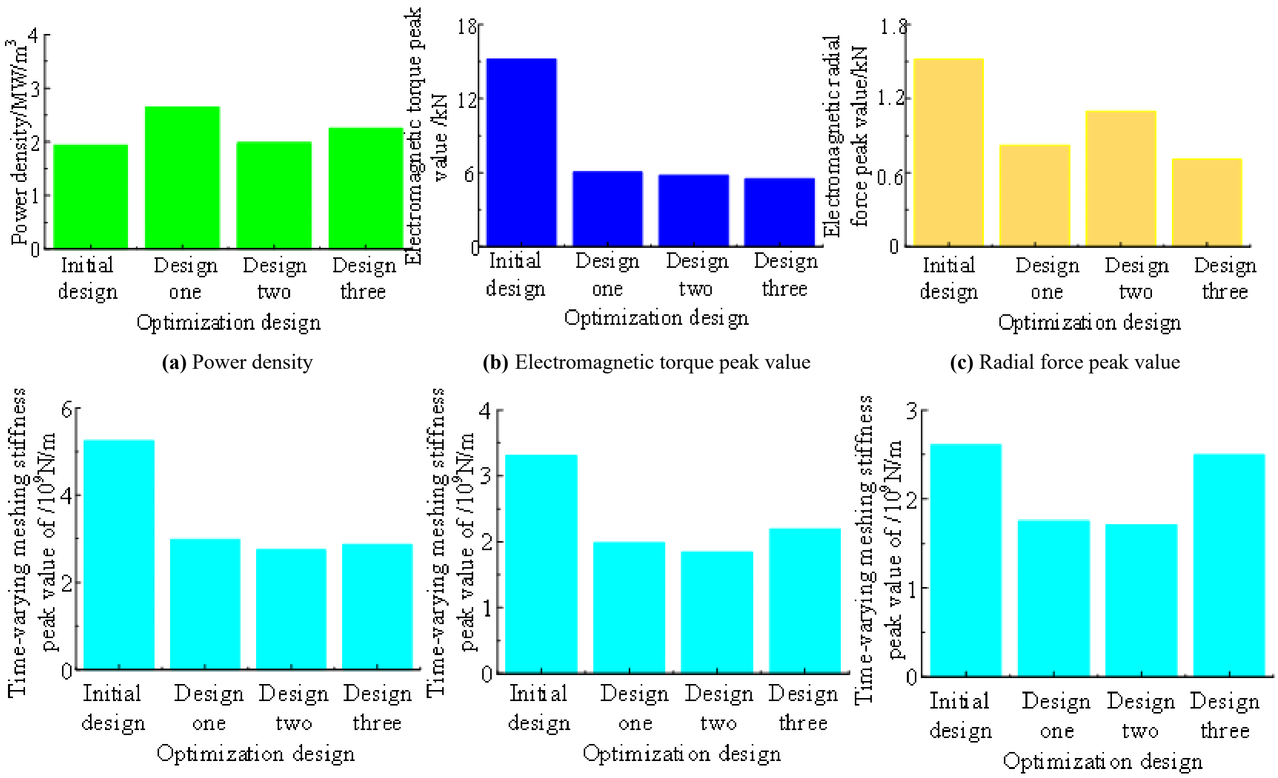

(a) Power density **(b)** Electromagnetic torque peak value **(c)** Radial force peak value

(d) Low-speed stage **(e)** Medium-speed stage **(f)** High-speed stage

Figure 7. Target value changes under various scenarios.

4. Dynamic performance-driven co-design of gearbox and generator parameters

4.1. Co-design process for second-level electromechanical parameters

Based on the optimal parameters of Stage 1 (Scheme 1), a refined electromechanical coupling dynamic model is used to analyze the influence of mechanical parameters (bearing stiffness, shaft size, spline size) and generator parameters (air-gap length, slot opening size, pole pitch) on system dynamic responses.

The workflow is shown in **Figure 8**. Sensitive parameters are determined by correlation analysis. Optimal Latin hypercube sampling (OLHS) is used to generate training and test samples. A Kriging meta-model is constructed to improve optimization efficiency. Finally, the NSGA-II algorithm is used to perform multi-objective optimization for vibration suppression and load attenuation.

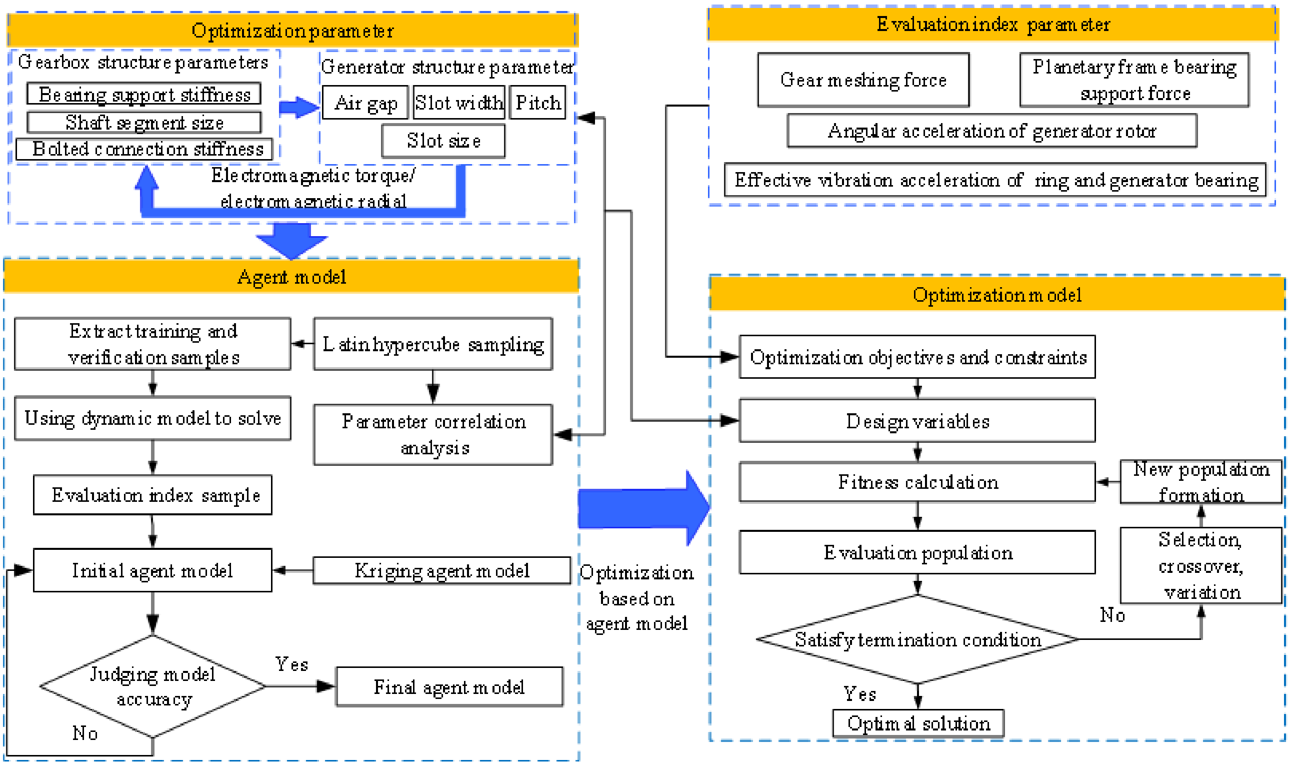

Figure 8. Dynamic performance optimization procedure based on a surrogate model.

4.2. Impact of electromechanical parameters on dynamic behavior

Based on the first-level integrated electromechanical design (Scheme 1), a correlation analysis was performed to evaluate the influence of gear system and generator parameters on gear dynamic loads, bearing support forces, and component vibration characteristics. Employing the refined electromechanical coupling dynamic model of the drive chain developed in Chen et al. [32], this study analyzes how electromechanical parameters affect system dynamic performance. The analysis specifically addresses the effects of mechanical structural parameters—such as bearing support stiffness, hollow shaft dimensions, and spline size—as well as generator parameters, including stator slot geometry, slot opening size, and air gap length, on the dynamic response of the wind turbine drive train. To enhance computational efficiency, housing structural characteristics were omitted from the dynamic model in this section.

First, system response metrics were defined as performance indicators. In this study, these include the peak-to-peak values of system acceleration, dynamic meshing force, and bearing support reaction force. The specific performance evaluation metrics are summarized in **Table 4** below:

Table 4. Gearbox-generator system performance evaluation index.

Name	Symbols	Weight factor	Name	Symbols	Weight factor
Medium-speed ring vibration acceleration amplitude	P1	0.1	Medium-speed planet carrier bearing support force amplitude	P6	0.05
High-speed ring vibration acceleration amplitude	P2	0.1	High-speed planet carrier bearing support force amplitude	P7	0.1
Generator bearing vibration acceleration amplitude	P3	0.15	Generator bearing support force amplitude	P8	0.1
Generator rotor torsional acceleration amplitude	P4	0.15	Dynamic meshing force of medium-speed stage amplitude	P9	0.1
Low-speed planet carrier bearing support reaction amplitude	P5	0.05	Dynamic meshing force of high-speed stage amplitude	P10	0.1

4.2.1. Influence of structural parameters on system dynamics

The input parameters considered in this study encompass meshing, structural, support, and connection parameters. **Table 5** summarizes the identification indices, baseline values, and upper and lower bounds for each parameter. An orthogonal experimental design was employed, with each variable uniformly sampled at 25 distinct levels to perform the computations.

Table 5. Input design variables of the transmission system.

Input parameter	Name	Symbol	Unit	Initial value	Upper and lower limits
Structural parameter	Low-speed sun gear outside diameter	x_1	m	0.72	[0.32, 0.96]
	Low-speed sun gear inner diameter	x_2	m	0.35	[0.13, 0.53]
	Medium-speed sun gear outside diameter	x_3	m	0.64	[0.2, 0.6]
	Medium-speed sun gear inner diameter	x_4	m	0.25	[0.06, 0.32]
	Generator rotor outside diameter	x_5	m	0.6	[0.25, 0.75]
	Generator rotor inner diameter	x_6	m	0.3	[0.1, 0.4]
Join parameter	Medium speed stage planet carrier spline connection outside diameter	x_7	m	0.7	[0.35, 1.05]
	Medium-speed stage planet carrier spline connection inner diameter	x_8	m	0.4	[0.14, 0.6]
	High-speed stage planet carrier spline connection outside diameter	x_9	m	0.65	[0.32, 0.98]
	High-speed stage planet carrier spline connection inner diameter	x_{10}	m	0.4	[0.13, 0.5]
	Low-speed ring gear bolt connection stiffness	x_{11}	N/m	9×10^{11}	[8×10^{10}, 1.6×10^{12}]
	Medium speed ring gear bolt connection stiffness	x_{12}	N/m	8×10^{11}	[5×10^{10}, 1×10^{12}]
	High-speed ring gear bolt connection stiffness	x_{13}	N/m	7×10^{11}	[4×10^{10}, 8×10^{11}]
Low speed stage	Planet carrier bearing support stiffness	x_{14}	N/m	1×10^{11}	[4×10^{10}, 2.4×10^{12}]
	Planet gear bearing support stiffness	x_{15}	N/m	7×10^{8}	[1×10^{8}, 4.2×10^{9}]
Medium speed stage	Planet carrier bearing support stiffness	x_{16}	N/m	9×10^{10}	[6×10^{9}, 3.6×10^{11}]
	Planet gear bearing support stiffness	x_{17}	N/m	6.05×10^{9}	[6.05×10^{8}, 3.6×10^{10}]
High-speed stage	Planet carrier bearing support stiffness	x_{18}	N/m	5.6×10^{10}	[2×10^{9}, 1.2×10^{11}]
	Planet gear bearing support stiffness	x_{19}	N/m	2×10^{9}	[2×10^{8}, 1.2×10^{10}]
Generator	Bearing support stiffness	x_{20}	N/m	1.9×10^{9}	[9×10^{7}, 5.4×10^{9}]

To quantitatively assess the influence of variations in structural parameters on dynamic performance metrics, the correlation coefficient R_{xy} for each parameter was computed using Equation (16). Values of R_{xy} closer to 1 indicate a stronger association between the structural parameter and the system performance. A correlation coefficient greater than or less than 0 indicates a positive or negative correlation, respectively.

$$R_{xy} = \frac{\sum (X_i - \overline{X}_i)(Y_i - \overline{Y}_i)}{\sqrt{\sum (X_i - \overline{X}_i)^2}\sqrt{\sum (Y_i - \overline{Y}_i)^2}}. \tag{16}$$

Where Y_i represents performance index, X_i represents structural parameter.

Figure 9 shows the top ten structural parameters by their correlation with the generator rotor's translational and torsional accelerations. The analysis shows that the generator rotor outer diameter (x_5), the bearing support stiffness of the high-speed-stage planet gear (x_{19}), and that of the medium-speed-stage planet gear (x_{17}) emerged as the most influential parameters.

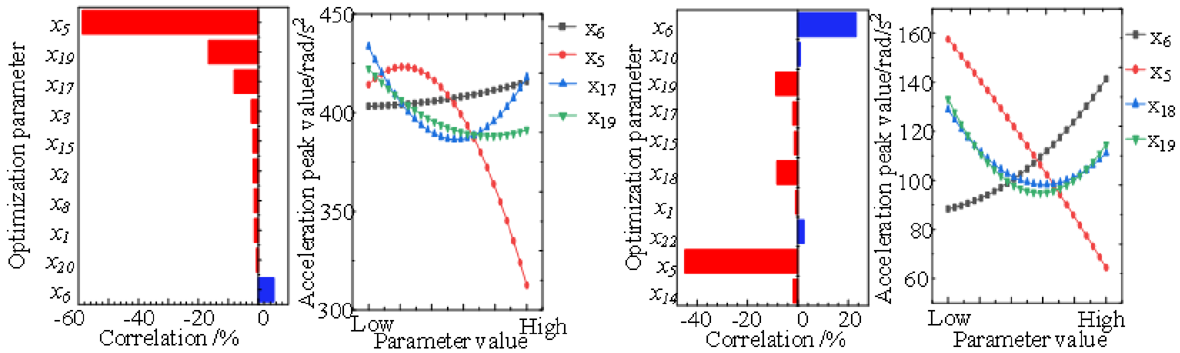

(a) Torsional angular acceleration **(b)** Peak value of vibration acceleration

Figure 9. Correlation analysis on angular and vibration acceleration of the generator rotor.

Figure 10 shows the correlation analysis of different structural parameters with the vibration acceleration of the medium- and high-speed stage internal ring gears. It can be seen that the key parameters affecting the vibration performance are the bolt connection stiffness of the internal ring gears at each stage (x_{12}, x_{13}) and the support stiffness of the planetary gear bearings at each stage (x_{17}, x_{19}).

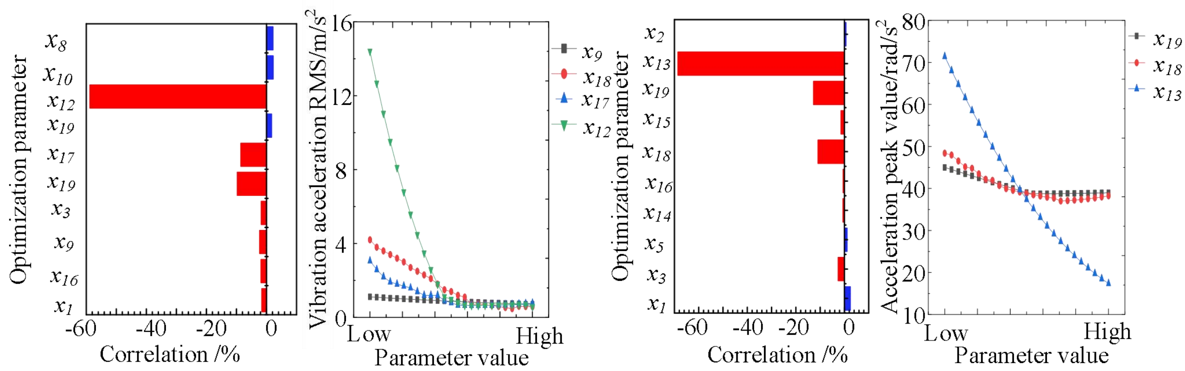

(a) Vibration acceleration of medium speed ring gear **(b)** Vibration acceleration of high speed ring gear

Figure 10. Correlation analysis on vibration acceleration of ring gear.

Figure 11 shows the correlation analysis between various mechanical structural parameters and the peak-to-peak dynamic meshing forces at the high- and medium-speed stages. The results indicate that the dominant parameters influencing the high-speed stage dynamic meshing forces are the bearing support stiffness of the high-speed planet gear (x_{18}), the carrier bearing support stiffness (x_{19}), and the outer diameter of the generator rotor shaft segment (x_5). For the medium-speed stage, the key influencing parameters are the bearing support stiffness of the medium-speed planet gear (x_{17}), the carrier bearing support stiffness (x_{16}), and the outer diameter of the medium-speed sun gear shaft segment (x_3). Regarding bearing support reactions, the generator bearing force is primarily affected by the bearing support stiffness of the high-speed planet gear (x_{19}), the carrier bearings (x_{18}), the generator bearings (x_{20}), and the outer diameter of the generator rotor shaft (x_5). The bearing support reaction force on the medium-speed carrier is mainly influenced by the outer diameter of the low-speed sun gear shaft (x_1) and the bearing support stiffness of the medium-speed planet gear (x_{16}), medium-speed carrier (x_{17}), and high-speed carrier (x_{18}).

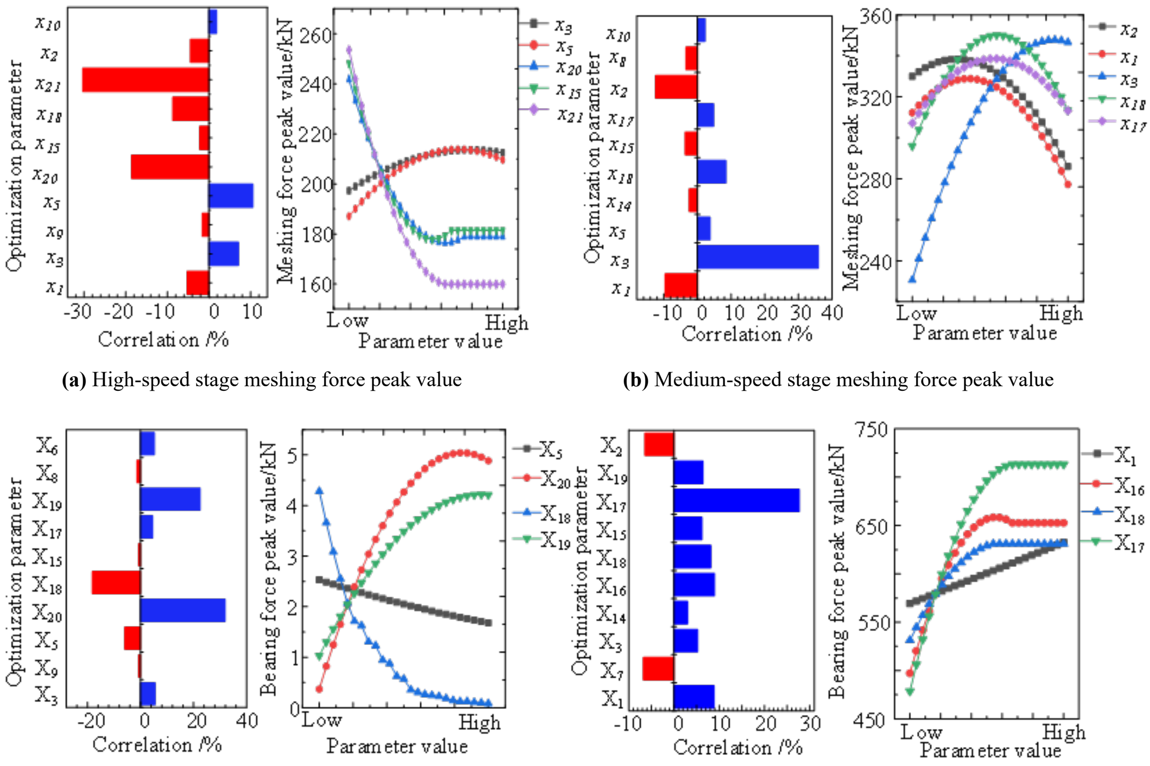

(a) High-speed stage meshing force peak value **(b)** Medium-speed stage meshing force peak value

(c) Generator bearing support force **(d)** Medium speed planet carrier bearing support force

Figure 11. Correlation analysis between mechanical structural parameters and meshing forces and bearing forces.

4.2.2. Influence of generator structural parameters on system dynamic performance

While maintaining constant operational performance of the permanent magnet generator—that is, ensuring that the output power and average electromagnetic torque satisfy the prescribed constraints—a correlation analysis was carried out to evaluate the influence of key generator structural parameters on system dynamic performance. The value ranges for each structural parameter are provided in **Table 6** below.

Table 6. Design variables and their ranges for the electrical machine system.

Input parameter	Symbol	Unit	Initial value	Upper and lower limits
Pitch	x_1	-	9	[1, 12]
Air gap	x_2	mm	8.5	[2, 15]
Slot width	x_3	mm	16.5	[1, 30]
Opening slot width	x_4	mm	19.1	[2, 19.1]
Stator core back width	x_5	mm	86.7	[50, 160]
Tooth slot depth	x_6	mm	18	[1, 40]

Figure 12 presents the correlation between generator structural parameters and the torsional and translational vibration accelerations of the generator rotor. The results indicate that the rotor vibration performance is predominantly influenced by the generator air gap length (x_2), pole pitch (x_1), and slot width (x_3).

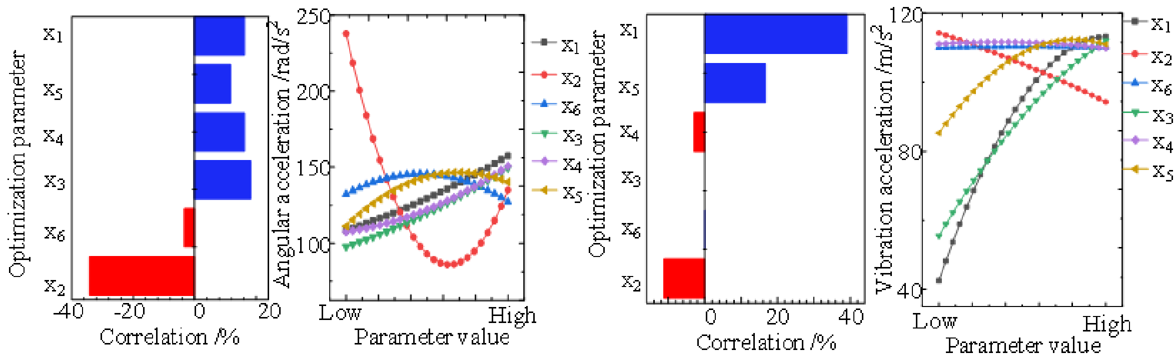

(a) Angular torsional acceleration **(b)** Vibration acceleration

Figure 12. Correlation analysis on vibration acceleration of generator rotor.

Figure 13 shows the correlation of generator structural parameters with the peak-to-peak dynamic meshing forces at the medium- and high-speed stages. It can be observed that the dynamic meshing forces and bearing support reaction forces are mainly affected by the generator air gap length (x_2), pole pitch (x_1), slot width (x_3), and stator core back width (x_5).

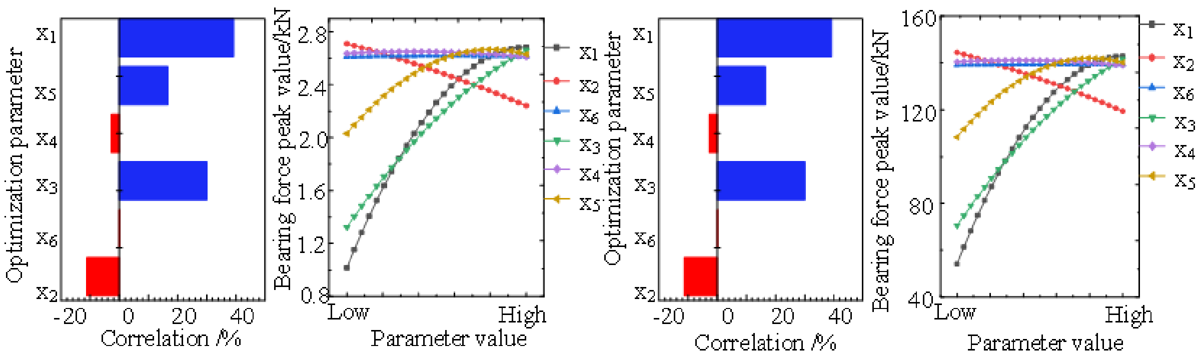

(a) Generator bearing support force **(b)** high speed planet carrier bearing support force

Figure 13. Correlation analysis of electrical machine parameters with meshing forces and bearing forces.

4.3. Development of a Kriging surrogate model and optimization objectives

The dynamic performance optimization of the wind turbine generator drive system aims to reduce vibration intensity across components, minimize fluctuations in dynamic meshing forces, and decrease bearing support reaction forces. The specific optimization criteria are summarized in **Table 4**, while the parameters and constraint ranges for the multi-objective optimization of the integrated gearbox–generator system are provided in **Table 7**. The corresponding objective functions and constraints are mathematically formulated as follows:

$$\begin{cases} \text{vars: X} = [X_1,\text{X}_2, X_3, X_4, X_5, ..., X_{15},\text{X}_{16}] \\ \text{min: F}(X) = w_1 \dfrac{F_{P1}(X)}{sf_{p1}} + w_2 \dfrac{F_{P2}(X)}{sf_{p2}} + w_3 \dfrac{F_{P3}(X)}{sf_{p3}} + w_4 \dfrac{F_{P4}(X)}{sf_{p4}} + w_5 \dfrac{F_{P5}(X)}{sf_{p5}} \\ \qquad + w_6 \dfrac{F_{P6}(X)}{sf_{p6}} + w_7 \dfrac{F_{P7}(X)}{sf_{p7}} + w_8 \dfrac{F_{P8}(X)}{sf_{p8}} + w_9 \dfrac{F_{P9}(X)}{sf_{p9}} + w_{10} \dfrac{F_{P10}(X)}{sf_{p10}} \\ s.t.:\ lb \le X \le ub \\ 8 \times 10^6 \le mean(Power) \le 8.75 \times 10^6 \\ 1.0 \times 10^5 \le mean(T_e) \le 1.7 \times 10^5 \end{cases}, \tag{17}$$

where $F_{Pi}(X)$ represents the objective function, sf_{pi} represents the scale factor, w_i represents the target weight, $mean(Power)$ represents the average output power of a generator under rated operating conditions, $mean(T_e)$ represents the average electromagnetic torque under rated operating conditions.

Table 7. Integrated system optimization variables.

	Optimization variable	Symbols	Value range
Gearbox structure parameter	Sun gear outside diameter (low speed, medium speed)/m	X_1, X_2	Refer to **Table 5**
	Outside diameter of generator rotor/m	X_3	
	Ring gear connection stiffness(low, medium and high speed)/N/m	$X_4, X_5, X_6,$	
	Planet carrier bearing stiffness (low speed, high speed)/N/m	$X_7, X_8,$	
	Planet gear bearing stiffness(medium, high speed)/N/m	X_9, X_{10}	
	Generator bearing support stiffness/N/m	X_{11}	
Generator structure parameter	Pitch	X_{12}	Refer to **Table 6**
	Air gap/mm	X_{13}	
	Slot width/mm	X_{14}	
	Stator core back width/mm	X_{15}	

The accuracy of a surrogate model is strongly influenced by the distribution and quantity of sample points in the design space. A sufficient number of uniformly distributed samples can effectively capture the global behavior of the actual system. In this study, the optimal Latin hypercube sampling (OLHS) method was employed to generate sample points. OLHS is a stratified sampling technique that ensures full coverage of all variable ranges with minimal samples, as described in He [33]. Sampling was performed within the predefined bounds of the design variables, with the additional requirement that all samples satisfy the specified constraint conditions. **Figure 14** shows the distribution of variable samples after random sampling and constraint application. A total of 640 sample points were generated using the OLHS method. Among these, 600 points were selected as training samples via the maximum discrepancy method (shown as blue squares), and the remaining 40 points were reserved for testing (marked as red stars).

In this paper, the Kriging method is selected to establish a surrogate model for the system. This method exhibits good continuity and differentiability due to its correlation function, providing excellent local estimation capabilities and a better approximation effect for nonlinear complex problems. The Kriging method is a type of interpolation method that predicts unknown observation points based on known points. The accuracy of the Kriging surrogate model can be evaluated using the coefficient of determination

(R^2). The closer (R^2) is to 1, the higher the similarity between the surrogate model and the original model. **Figure 15** shows the (R^2) values of the Kriging surrogate model for the system evaluation indicators. As shown in the figure, the (R^2) values under the Kriging surrogate model are all greater than 0.9, indicating that the model has good nonlinear fitting ability, and the fitting accuracy meets the optimization requirements,

$$\begin{cases} \mathrm{R}^2 = 1 - \dfrac{\mathrm{SSE}}{\mathrm{SST}} \\ \mathrm{SSE} = \sum_{\mathrm{i}=1}^{\mathrm{n}} (\mathrm{y_i} - \widetilde{\mathrm{y}}_\mathrm{i})^2 \\ \mathrm{SST} = \sum_{\mathrm{i}=1}^{\mathrm{n}} (\mathrm{y_i} - \overline{\mathrm{y}})^2 \end{cases}, \tag{18}$$

where $\widetilde{y}_i$ represent the predicted value of the ith response, y_i represent the true value of the ith response, $\bar{y}_i$ represent the mean true value of the response, and n represent the number of data points used to test the accuracy of the model.

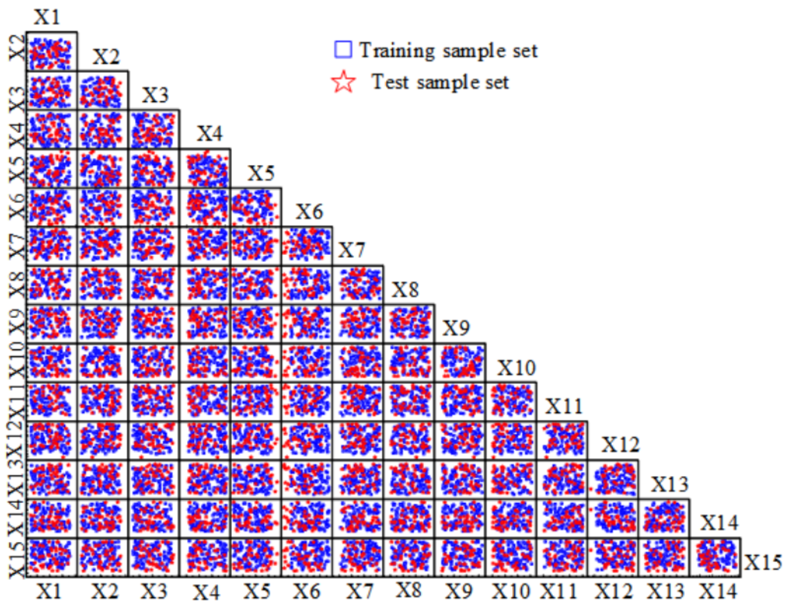

Figure 14. Variable sample space filling diagram.

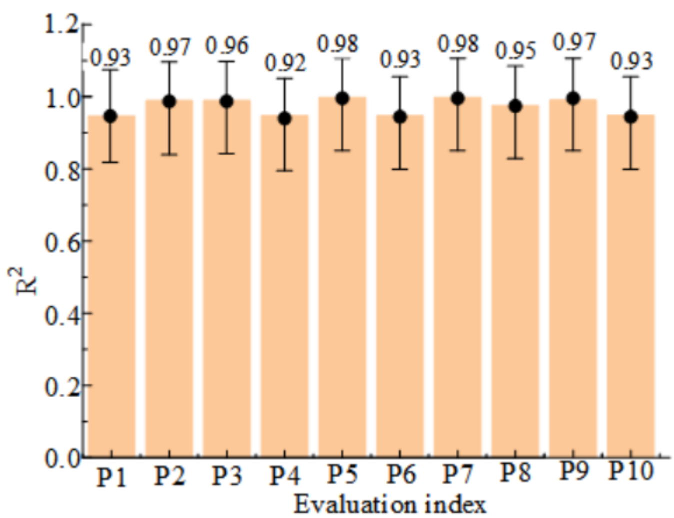

Figure 15. Determination coefficient R^2.

4.4. Multi-objective optimization and results using surrogate models

The NSGA-II algorithm is used with crossover probability 0.5, population size 100, maximum iterations 200, and fitness deviation 0.01. The Pareto solution sets of dynamic indices are shown in **Figure 16**. The solution closest to the ideal point is selected as the optimal dynamic design, with key parameters listed in **Table 8**.

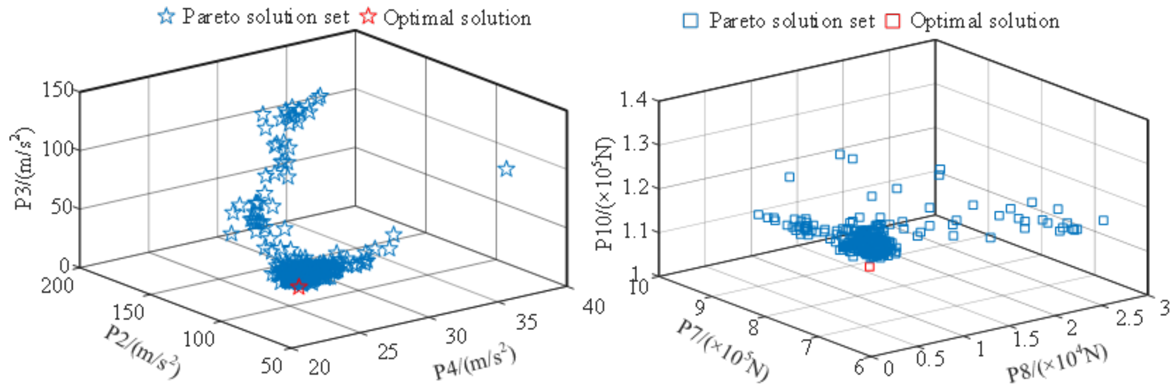

(a) Effective value index of acceleration **(b)** Effective value index of meshing and bearing support force

Figure 16. Pareto solution set of dynamic performance evaluation index.

Table 8. Dynamic performance optimum parameter.

	Optimization variable	**Initial parameter**	**Optimized design**
Gearbox structure parameter	Sun gear outside diameter (low speed, medium speed)/m	0.72, 064	0.6423, 0.4325
	Outside diameter of generator rotor/m	0.6	0.54867
	Ring gear connection stiffness(low, medium and high speed)/N/m	9×10^{11}, 8×10^{11}, 7×10^{11}	8.25×10^{11}, 5.4×10^{11}, 4.62×10^{11}
	Planet carrier bearing stiffness (low speed, high speed)/N/m	9×10^{10}, 5×10^{10}	6.2589×10^{10}, 2.6534×10^{10}
	Planet gear bearing stiffness (medium and high speed)/N/m	6.05×10^{9}, 2×10^{9}	9.628×10^{8}, 8.44×10^{8}
	Generator bearing support stiffness/N/m	3×10^{9}	9.96×10^{8}
Generator structure parameter	Pitch	9	8
	Air gap/mm	8.5186	7.5
	Slot width/mm	16.529	14.1
	Stator core back width/mm	86.559	75

4.5. Dynamic performance optimization results

The optimized parameters were applied to the dynamic model of the integrated wind turbine gearbox-generator system to validate the improvement in dynamic performance. A comparison of the system dynamic response under steady-state rated wind speed conditions before and after optimization is presented in **Figure 17**. The results demonstrate a notable enhancement in the dynamic response of the bearing support reaction forces. Specifically, both the root mean square and peak-to-peak values of the windward bearing reaction forces on the high- and medium-speed carriers decreased significantly. Improvements are also evident in the dynamic meshing behavior at the high-speed stage, where issues such as tooth disengagement and back-side contact have been effectively mitigated. Furthermore, vibration characteristics show marked improvement, with substantial reductions in vibration acceleration levels observed at the internal gears of the high- and medium-speed stages, as well as at the generator bearings.

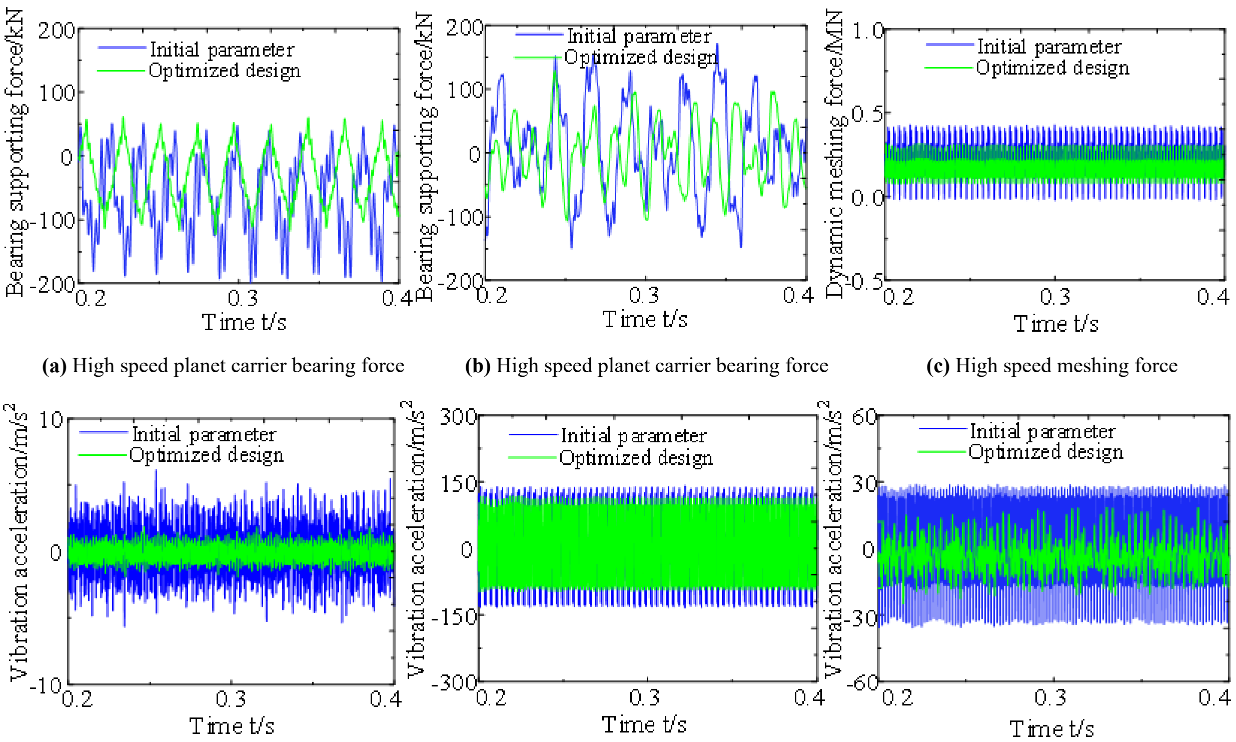

(a) High speed planet carrier bearing force **(b)** High speed planet carrier bearing force **(c)** High speed meshing force

(d) Middle speed ring gear **(e)** Generator bearing **(f)** High speed ring gear

Figure 17. Comparison of system dynamic responses before and after optimization under steady-state conditions.

Figure 18 shows the dynamic response characteristics of wind turbine system components before and after optimization under variable speed and load conditions. As shown, the peak-to-peak values of the dynamic responses generally increase with wind speed, accompanied by noticeable resonance phenomena. From **Figure 18a**,**b**, the peak-to-peak dynamic meshing forces at each stage are significantly reduced. Under variable operating conditions, the average reductions in these values are 14% for the medium-speed stage and 26.7% for the high-speed stage. Dynamic load improvement is particularly evident under high-speed heavy-load and resonant conditions, where the original potential resonance region A is eliminated. It should be noted, however, that a new resonance region B emerges in the optimized system, though the overall dynamic performance of the gear system is substantially improved. In Region B, the peak vibration acceleration of the high-speed ring gear is approximately 12.5 m/s^2, which is below the alarm threshold (typically 25 m/s^2) specified in ISO 10816-3 for wind turbine drivetrains. **Figure 18c** shows the dynamic response of the bearing support reaction forces on the high-speed carrier. The root-mean-square and peak-to-peak values are markedly reduced, with an average improvement of 48% under variable conditions, effectively eliminating the original resonance region C. **Figure 18d**–**f** compare the vibration characteristics of structural components. Under high-speed heavy-load conditions, the optimized design reduces component vibration intensity, thereby improving overall system vibration performance. The most significant improvements are observed in the vibration intensity of the medium-speed internal ring gear and the generator rotor.

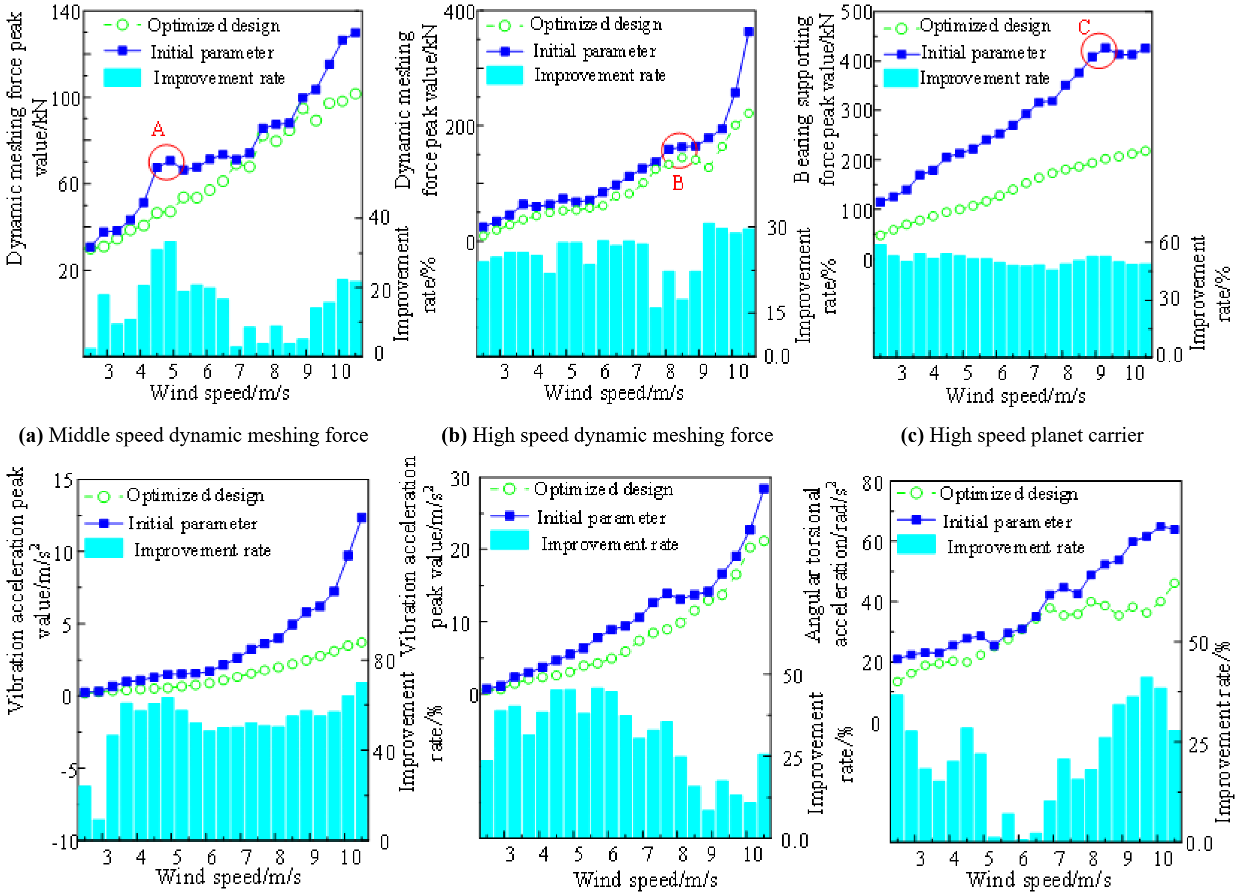

(a) Middle speed dynamic meshing force **(b)** High speed dynamic meshing force **(c)** High speed planet carrier

(d) Middle speed ring gear **(e)** High speed ring gear **(f)** Generator rotor

Figure 18. Comparison of dynamic responses before and after optimization under variable speed and load conditions.

5. Conclusion

Aiming at boosting power density and attenuating dynamic loads and vibrations of wind turbine drivetrains, this paper proposes a two-level hierarchical mechatronic co-design method for wind turbine gearbox–generator systems, which breaks through the limitations of traditional decoupled design and achieves synchronous improvement of power density and dynamic performance. The main conclusions are as follows:

(1) A multi-level integrated design methodology for the electromechanical parameters of the wind turbine drive train was developed. At the first level, the initial parameters of the gearbox–generator system were designed to improve the overall power density while minimizing the peak-to-peak values of internal excitations, such as gear time-varying mesh stiffness and generator pulsating electromagnetic torque. Using these results as initial inputs for the second level, a correlation analysis between mechanical/generator structural parameters and system dynamic performance was conducted based on an electromechanical coupling dynamics model. Key sensitive parameters were identified, and a Kriging surrogate model was constructed. With dynamic load and vibration performance as comprehensive objectives, an optimal set of parameters was

determined near the second-level initial values, resulting in an optimized integrated design for the drive train.

(2) The first-level integrated electromechanical parameter design achieved a balanced optimization of the gearbox and generator structural parameters under their respective design constraints. Using the NSGA-II non-dominated sorting genetic algorithm and the resulting Pareto-optimal set, a design scheme with optimal performance indicators was obtained. Compared to the original design, the integrated approach increased the power density by 35%, reduced the peak-to-peak electromagnetic torque and radial force by 54% and 47%, respectively, and decreased the peak-to-peak time-varying mesh stiffness by 43%, 57%, and 32% for the low-, medium-, and high-speed stages.

(3) A sensitivity analysis of the electromechanical structural parameters revealed that the dynamic behavior of the coupled system is significantly influenced by the support stiffness of planetary gears at different stages, the bolt connection stiffness of ring gears, and the outer diameters of shaft segments. In the generator, parameters such as air gap length, pole pitch, slot width, and stator core back width also considerably affect system dynamics. These insights helped identify the key sensitive parameters for the second-level optimization.

(4) For the second-level integrated design, a Kriging surrogate model was constructed and combined with the NSGA-II algorithm to optimize the electromechanical structural parameters, using the dynamic response of each component under rated conditions as the objective. The optimized design effectively reduced dynamic gear and bearing loads, prevented tooth disengagement and back-side contact, and improved component vibration performance. Further analysis under variable speed and load conditions confirmed that the proposed design achieves vibration and load reduction across the entire operating range of the wind turbine drive system.

Limitations: The electromechanical co-design presented herein has several idealized assumptions and limitations. The coupling dynamic model assumes perfect gear alignment, constant temperature, and neglects housing flexibility, whereas in reality, wind turbines inevitably suffer from manufacturing errors, thermal deformations, and nacelle frame vibrations. Furthermore, the optimization does not include thermal constraints (e.g., generator cooling, gear scuffing, oil film temperature rise) nor centrifugal stress limits for high-speed rotors. Extreme transient events such as grid faults and emergency stops are also not considered. Future work should integrate thermal-structural-electromagnetic simulations, include transient fault scenarios, and ultimately perform experimental validation to bridge the gap between these simulation-based results and real-world applications.

Author contributions: Conceptualization, RC and DQ; software, RC; writing—original draft preparation, RC; methodology, ZW; validation, ZW; formal analysis, CZ; visualization, CZ; resources, JS; data curation, RC and JS. All authors have read and agreed to the published version of the manuscript.

Funding: This research received no external funding

Institutional review board statement: Not applicable.

Informed consent statement: Not applicable.

Data availability statement: No new data were created or analyzed in this study. Data sharing is not applicable to this article.

Conflict of interest: The authors declare no conflict of interest.

AI use statement: During the preparation of this manuscript, the authors used DeepSeek solely for language refinement. No AI tools were used for data analysis, interpretation, or generation of scientific content. All outputs were critically reviewed and edited by the authors. The authors take full responsibility for the integrity and accuracy of the work.

References

1. Rubio F, Llopis-Albert C, Pedrosa AM. Analysis of the Influence of Calculation Parameters on the Design of the Gearbox of a High-Power Wind Turbine. Mathematics. 2023; 11(19): 4137. doi: 10.3390/math11194137
2. Llopis-Albert C, Rubio F, Devece C, et al. Digital Twin-Based Approach for a Multi-Objective Optimal Design of Wind Turbine Gearboxes. Mathematics. 2024; 12(9): 1383. doi: 10.3390/math12091383
3. Wang C. Study on dynamic performance and optimal design for differential gear train in wind turbine gearbox. Renewable Energy. 2024; 221: 119776. doi: 10.1016/j.renene.2023.119776
4. Bußkamp P, Jacobs G, Röder J. Multiobjective wind turbine gearbox design optimization to reduce component damage risk during grid faults. Forschung im Ingenieurwesen. 2025; 89(1): 48. doi: 10.1007/s10010-025-00821-2
5. Zhou L, An X, Chen H. Multi-objective Optimization Design of Gearbox with Helical Cylindrical Gear Drive. Journal of Mechanical Transmission. 2016; 40(3): 62–65. Available online: https://www.jxcd.net.cn/thesisDetails#10.16578/j.issn.1004.2539.2016.03.013&lang=zh (in Chinese)
6. Savsani V, Rao RV, Vakharia DP. Optimal weight design of a gear train using particle swarm optimization and simulated annealing algorithms. Mechanism and Machine Theory. 2010; 45(3): 531–541. doi: 10.1016/j.mechmachtheory.2009.10.010
7. Gologlu C, Zeyveli M. A genetic approach to automate preliminary design of gear drives. Computers & Industrial Engineering. 2009; 57(3): 1043–1051. doi: 10.1016/j.cie.2009.04.006
8. Chen J, Wu S, Hsieh C. Design of optimal weight for a gear transmission system using hybrid taguchi-genetic algorithm. Wuhan University Journal of Natural Sciences. 2012; 17(4): 331–336. (in Chinese)
9. Wei J, Yang P, Qin D, et al. Equal-strength optimization design method for heavy-duty planetary gear transmissions. Journal of Beijing University of Technology. 2018; 44(7): 979–986. Available online: https://journal.bjut.edu.cn/bjgydxxb/cn/article/doi/10.11936/bjutxb2017050047 (in Chinese)
10. Liang M, Hu J, Li S, et al. Topology optimization of transmission gearbox under multiple working loads. Advances in Mechanical Engineering. 2018; 10(11). doi: 10.1177/1687814018813454
11. Lv X, Ruan X, Zhong J, et al. Study on Design of Elastic Support for Wind Turbine. E3S Web of Conferences. 2020; 194: 03017. doi: 10.1051/e3sconf/202019403017
12. Lei Y, Hou L, Fu Y, et al. Research on vibration and noise reduction of electric bus gearbox based on multi-objective optimization. Applied Acoustics. 2020; 158: 107037. doi: 10.1016/j.apacoust.2019.107037
13. Jouilel N, Radouani M, El Fahime B. Wind Turbine's Gearbox Aided Design Approach Using Bond Graph Methodology and Monte Carlo Simulation. International Journal of Precision Engineering and Manufacturing-Green Technology. 2021; 8(1): 89–101. doi: 10.1007/s40684-019-00170-w
14. Bozca M. Transmission error model-based optimisation of the geometric design parameters of an automotive transmission gearbox to reduce gear-rattle noise. Applied Acoustics. 2018; 130: 247–259. doi: 10.1016/j.apacoust.2017.10.005
15. Garambois P, Perret-Liaudet J, Rigaud E. NVH robust optimization of gear macro and microgeometries

using an efficient tooth contact model. Mechanism and Machine Theory. 2017; 117: 78–95. doi: 10.1016/j.mechmachtheory.2017.07.008

16. Liu G, Liu H, Zhu C, et al. Design optimization of a wind turbine gear transmission based on fatigue reliability sensitivity. Frontiers of Mechanical Engineering. 2021; 16(1): 61–79. doi: 10.1007/s11465-020-0611-5
17. Zhang Y, Ji JC, Ren Z, et al. Digital twin-driven partial domain adaptation network for intelligent fault diagnosis of rolling bearing. Reliability Engineering & System Safety. 2023; 234: 109186. doi: 10.1016/j.ress.2023.109186
18. Liu X, Jiang D, Tao B, et al. A systematic review of digital twin about physical entities, virtual models, twin data, and applications. Advanced Engineering Informatics. 2023; 55: 101876. doi: 10.1016/j.aei.2023.101876
19. Zhou Y, Zhou J, Cui Q, et al. Digital twin-driven online intelligent assessment of wind turbine gearbox. Wind Energy. 2024; 27(8): 797–815. doi: 10.1002/we.2912
20. Öztürk N, Dalcalı A, Çelik E, et al. Cogging torque reduction by optimal design of PM synchronous generator for wind turbines. International Journal of Hydrogen Energy. 2017; 42(28): 17593–17600. doi: 10.1016/j.ijhydene.2017.02.093
21. Abdoos A, Moazzen ME, Ebadi A. Optimal Design of a Radial-Flux Permanent Magnet Generator with Outer-Rotor for Direct-Drive Wind Turbines. Computational Intelligence in Electrical Engineering. 2020; 11(4). doi: 10.22108/isee.2020.117057.1227 (in Persian)
22. Alemi-Rostami M, Rezazadeh G, Alipour-Sarabi R, et al. Design and Optimization of a Large-Scale Permanent Magnet Synchronous Generator. Scientia Iranica. 2019; 29(1). doi: 10.24200/sci.2019.53569.3314
23. Jin F, Si J, Cheng Z, et al. Optimization Design of A Novel Toroidal-Winding Permanent Magnet Synchronous Generator. In: Proceedings of the 2019 22nd International Conference on Electrical Machines and Systems (ICEMS); 11–14 August 2019; Harbin, China. pp. 1–5. doi: 10.1109/ICEMS.2019.8921858
24. Emami SP, Mahmoudi A, Kahourzade S. Robust Optimization of a Wind Generator based on an Analytical Model and Wind data of a Site. In: Proceedings of the 2020 IEEE International Conference on Power Electronics, Drives and Energy Systems (PEDES); 16–19 December 2020; Jaipur, India. pp. 1–6. doi: 10.1109/PEDES49360.2020.9379720
25. Mohd-Shafri SA, Tiang TL, Ishak D, et al. Optimal Design of SMPMSM Using Genetic Algorithm Based on Finite Element Model. In: Proceedings of the 11th International Conference on Robotics, Vision, Signal Processing and Power Applications. Springer; 2022. pp. 721–726. doi: 10.1007/978-981-16-8129-5_110
26. Mohd-Shafri SA, Tiang TL, Tan CJ, et al. Optimal Design of SMPMSM Using SD-model based on Genetic Algorithm. In: Proceedings of the 2021 IEEE International Magnetic Conference (INTERMAG); 26–30 April 2021; Lyon, France. pp. 1–7. doi: 10.1109/INTERMAG42984.2021.9579622
27. Sindhya K, Manninen A, Miettinen K, et al. Design of a Permanent Magnet Synchronous Generator Using Interactive Multiobjective Optimization. IEEE Transactions on Industrial Electronics. 2017; 64(12): 9776–9783. doi: 10.1109/TIE.2017.2708038
28. Dang L, Samb SO, Bernard N. Design optimization of a direct-drive PMSG considering the torque-speed profile Application for Offshore wind energy. In: Proceedings of the 2020 International Conference on Electrical Machines (ICEM); 23–26 August 2020; Gothenburg, Sweden. pp. 1875–1881. doi: 10.1109/ICEM49940.2020.9271034
29. Dang L, Samb SO, Sadou R, et al. Co-Design Optimization of Direct Drive PMSGs for Offshore Wind Turbines Based on Wind Speed Profile. Energies. 2021; 14(15): 4486. doi: 10.3390/en14154486
30. Asef P, Perpina RB, Barzegaran MR, et al. Multiobjective Design Optimization Using Dual-Level Response Surface Methodology and Booth's Algorithm for Permanent Magnet Synchronous Generators. IEEE Transactions on Energy Conversion. 2018; 33(2): 652–659. doi: 10.1109/TEC.2017.2777397
31. Jaen-Sola P, McDonald AS, Oterkus E. Lightweight design of direct-drive wind turbine electrical generators: A comparison between steel and composite material structures. Ocean Engineering. 2019; 181: 330–341. doi: 10.1016/j.oceaneng.2019.03.053
32. Chen R, Qin D, Liu C. Dynamic modelling and dynamic characteristics of wind turbine transmission gearbox-generator system electromechanical-rigid-flexible coupling. Alexandria Engineering Journal. 2023; 65: 307–325. doi: 10.1016/j.aej.2022.10.036
33. He Y. Research on Uniformity and Orthogonality of Latin Hypercube Design [PhD Thesis]. Peking University; 2011. Available online: https://d.wanfangdata.com.cn/thesis/Y2024797 (in Chinese)